Microcanonical Analysis of the Kinetic Method. The Meaning of the "Apparent Entropy"

Kent M. Ervin
Department of Chemistry and Chemical Physics Program, University of Nevada, Reno, Nevada, USA

A rigorous analysis of the kinetic method is carried out using Rice-Ramsperger-Kassel-Marcus (RRKM) theory of microcanonical statistical unimolecular dissociation rates. The model employs a kinetics treatment appropriate for metastable ion dissociation. Proton-bound alkoxide dimer anions are used as model systems, with realistic vibrational and rotational parameters calculated by ab initio methods for the cluster ion and transition states leading to the competitive dissociation channels. The numerical simulations show that the kinetic method plots of $\ln(I_2/I_1)$ versus $\Delta\Delta H$ are nearly linear but can exhibit significant curvature. The apparent entropy obtained in the extended kinetic method is *not* approximately equal to the thermodynamic entropy difference for dissociation, $\Delta\Delta S(T)$, or for activation, $\Delta\Delta S^{\ddagger}(T)$, either at the effective temperature or at any fixed equilibrium temperature. Instead, the apparent entropy term can be related to the ratio of the microcanonical sum of states of the dissociation transition states for the kinetically selected internal energy of the dissociating ions. (J Am Soc Mass Spectrom 2002, 13, 435–452) © 2002 American Society for Mass Spectrometry

The kinetic method is a popular mass spectrometry technique for obtaining relative ion affinities. In the kinetic method, originally developed by Cooks and co-workers [1–4], the metastable or collision-induced decomposition of a mass-selected cluster ion that has two product channels is monitored in a tandem mass spectrometer. An example of an application of the kinetic method is shown in Figure 1, a schematic energy diagram of the dissociation of a proton-bound alkoxide/alkanol anion as in reactions 1 and 2.

$$[R_1O\text{—}H\text{—}OR_2]^- \rightarrow R_1O^- + R_2OH(\Delta_1H) \quad (1)$$

$$\rightarrow R_1OH + R_2O^- \ (\Delta_2H) \quad (2)$$

A correlation between the ratio of the intensities of the two product ions and the thermochemical enthalpy difference of the two product channels is made according to eq 3,

$$\ln \frac{I_2}{I_1} \approx -\frac{\Delta\Delta H}{RT_{\text{eff}}} + \frac{\Delta\Delta S}{R} \quad (3)$$

where I_j is the detected intensity of product ion R_jO^-, $\Delta\Delta H = \Delta_2H - \Delta_1H = \Delta_{\text{acid}}H(R_2OH) - \Delta_{\text{acid}}H(R_1OH)$, $\Delta\Delta S = \Delta_2S - \Delta_1S$,$R$ is the gas constant, and the effective temperature T_{eff} is a kinetic correlation parameter that is determined from a calibration plot of $\ln(I_2/I_1)$ versus $\Delta\Delta H$ (slope $= -1/RT_{\text{eff}}$). By measuring the product intensity ratios for proton-bound dimers composed of partners with known acidity, the slope of the correlation is found and then the acidity of an unknown can be measured versus a reference acid. Theoretical formulations of varying levels of sophistication have been given that justify the correlation given by eq 3 [1, 2, 5–12], but its use and the meaning of the effective temperature parameter are points of active discussion [4, 10, 11, 13–15].

In the "standard kinetic method" [4], the entropy term in eq 3, $\Delta\Delta S$, is assumed to be zero. The "extended kinetic method" [4] developed by Fenselau [16, 17], Wesdemiotis [18–20] and their co-workers employs different instrumental conditions to vary the effective temperature, then treats the effective temperature parameter as a thermodynamic temperature to extract apparent entropy differences, $\Delta\Delta S_{\text{app}}$, between pairs of cluster ions. Armentrout proposed an improved statistical treatment of extended kinetic method data to

Published online March 26, 2002

Dedicated to Professor Peter B. Armentrout, who greatly appreciates thermokinetic methods, in celebration of his many contributions to mass spectrometry and ion chemistry as recognized by the 2001 Biemann Medal and in thanks for his advice, support, and friendship over the years.

Address reprint requests to Dr. K. M. Ervin, Department of Chemistry, University of Nevada/216, Reno, NV 89557-0020, USA. E-mail: ervin@chem.unr.edu

1044-0305/02/$20.00
PII S1044-0305(02)00357-4

Received November 28, 2001
Revised January 23, 2002
Accepted January 23, 2002

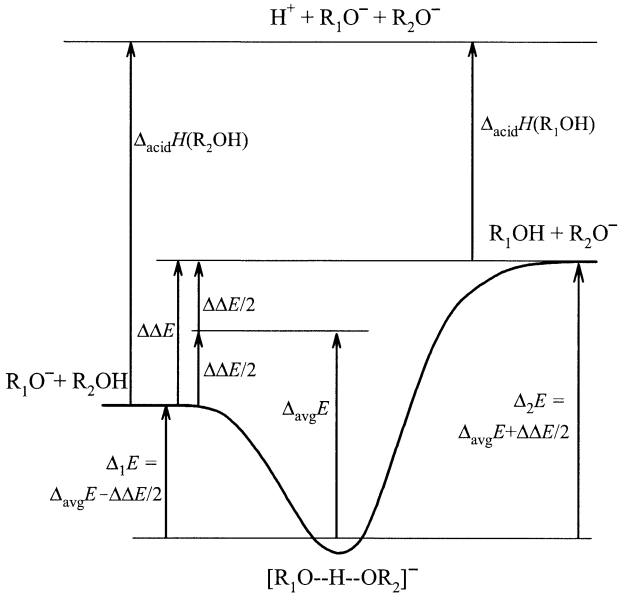

Figure 1. Schematic energy diagram of the dissociation of a proton-bound alkoxide/alkanol dimer anion.

obtain enthalpy differences and the apparent entropies with realistic uncertainties [21]. This "full entropy analysis" has been used for measurements of proton affinities and electron affinities [22–26] by the extended kinetic method. In their finite heat bath theory and RRKM theory simulations, Laskin and Futrell [9] found reasonable agreement between the apparent entropy and the thermodynamic entropy difference. However, there has been general conceptual criticism of using the effective temperature as a thermodynamic quantity to obtain entropy information [11, 13].

This work presents a rigorous analysis of the kinetic method using the microcanonical RRKM [27] theory of statistical unimolecular dissociation rates and a complete kinetics analysis suitable for metastable ion dissociation in a tandem mass spectrometer. Numerical simulations are applied to a series of model systems selected to elucidate aspects of the kinetic method that are critical for evaluation of thermochemical results from experiments including entropy effects. Simulations allow one to define the "true" molecular and energetic parameters exactly (without experimental uncertainty), and then determine whether the kinetic method measurements would yield back the same energetics. In simulations, molecular parameters can be varied artificially to gauge their effects. Proton-bound alkoxide/alkanol anions are used here as model systems to generate physically reasonable parameters via ab initio calculations and experimental data, but no attempt is made to model any actual experiments or real systems.

Canonical Formulation

The correlation of eq 3 was originally justified using canonical transition state theory [1, 2]. This derivation is repeated here in order to define terms and to discuss approximations. It is first assumed that the ratio of the ion intensities observed for the two channels is equal to the ratio of the macroscopic rate coefficients, as given by eq 4.

$$\frac{I_2}{I_1} \approx \frac{k_2(T)}{k_1(T)} \tag{4}$$

According to canonical transition state theory [28, 29], the reaction rate coefficients for the competing decomposition channels, $j = 1$ and 2, are given by eq 5,

$$k_j(T) = \frac{k_B T}{h} \frac{Q_j^{\ddagger}(T)}{Q_0(T)} e^{-\Delta_j E_0^{\ddagger}/RT} \tag{5}$$

where T is temperature, h is Planck's constant, k_B is Boltzmann's constant, $Q_j^{\ddagger}(T)$ is the partition function for the transition state leading to channel j, $Q_0(T)$ is the partition function for the cluster ion, and $\Delta_j E_0^{\ddagger}$ is the energy difference between the cluster and the transition state configuration at zero temperature. The rate coefficient, $k(T)$, strictly applies to a canonical ensemble of reactant molecules, i.e., reactants in thermodynamic equilibrium at temperature T.

Taking the logarithm of the ratio of the rate coefficients for the two channels, one obtains eq 6,

$$\ln \frac{k_2(T)}{k_1(T)} = -\frac{\Delta_2 E_0^{\ddagger} - \Delta_1 E_0^{\ddagger}}{RT} + \ln \frac{Q_2^{\ddagger}(T)}{Q_1^{\ddagger}(T)} \tag{6}$$

which contains no additional approximations beyond those of transition state theory [28, 29]. One combines eqs 4 and 6 and further assumes (1) either that the reverse activation energies are zero for both channels [$\Delta_j E_0^{\ddagger} \approx \Delta_j E_0$] or at least that the reverse activation energies are identical [$\Delta\Delta E_0^{\ddagger} \approx \Delta\Delta E_0$], (2) that the entropy differences between the two channels are zero [$\Delta\Delta S^{\ddagger}(T) = R \ln(Q_2^{\ddagger}/Q_1^{\ddagger}) \approx 0$] in the standard kinetic method or else that $\Delta\Delta S^{\ddagger}(T)$ is constant for various cluster ions in the extended kinetic method, and (3) that the integrated heat capacity differences between internal energy at 0 K and the enthalpy at various temperatures are equal for the two channels [$\Delta\Delta E_0 = \Delta_2 E_0 - \Delta_1 E_0 \approx \Delta\Delta H_T$]. With these approximations, one obtains eq 7,

$$\ln \frac{I_2}{I_1} = -\frac{\Delta\Delta H}{RT_{\text{eff}}} + \frac{\Delta\Delta S_{\text{app}}}{R} \tag{7}$$

where the substitutions $T \rightarrow T_{\text{eff}}$ and $\Delta\Delta S^{\ddagger}(T) \rightarrow \Delta\Delta S_{\text{app}}$ recognize that the clusters in an ion beam are isolated species, not in thermodynamic equilibrium at any temperature.

Fundamentally, the kinetic method and other thermokinetic methods work well for determining reaction energies or enthalpies because the rates in eqs 5 and 6

depend exponentially on the activation energies, but much more weakly on frequencies and molecular geometries as contained in the partition functions or entropy terms. Conversely, thermokinetic experiments are less sensitive to reaction entropies.

In this work, $\Delta\Delta S(T)$ and $\Delta\Delta S^{\ddagger}(T)$ represent the thermodynamic entropy difference between the two channels for isolated products and the dissociation transition states, respectively. The "thermodynamic" entropy refers here to the entropy for a canonical ensemble, which is associated with an Boltzmann energy distribution for systems in equilibrium at the temperature T. (Technically, other ensembles can be described by thermodynamics also.) From statistical mechanics, $\Delta\Delta S^{\ddagger}(T) = R \ln[Q_2^{\ddagger}(T)/Q_1^{\ddagger}(T)]$ and $\Delta\Delta S(T) = R \ln[Q_2(T)/Q_1(T)]$. Fenselau and co-workers [16, 17] and Wesdemiotis and co-workers [18–20] state that $\Delta\Delta S(T) = \Delta\Delta S^{\ddagger}(T)$ for cluster ions with zero reverse activation energies for dissociation. Researchers using the full entropy analysis method have equated the apparent entropy term either with the entropy difference for dissociation, $\Delta\Delta S(T)$, [21–24], or with the entropy difference for activation, $\Delta\Delta S^{\ddagger}(T)$ [26]. The assumption $\Delta\Delta S(T) = \Delta\Delta S^{\ddagger}(T)$ is also implicit in implementations of the kinetic method that calibrate against Gibbs energies instead of enthalpies, i.e., $\ln(I_2/I_1) = -\Delta\Delta G/RT_{\text{eff}}$ instead of eq 7.

To examine the $\Delta\Delta S(T) = \Delta\Delta S^{\ddagger}(T)$ assumption in detail, consider a barrierless dissociation process characterized by a loose transition state where the vibrational frequencies and internal rotational constants of the transition states are identical to those of the products and where the transition state is located at the centrifugal barrier for dissociation [30]. Then $\Delta\Delta S_{\text{vib}}(T) = \Delta\Delta S_{\text{vib}}^{\ddagger}(T)$ is exactly true for the vibrational contributions to the entropy differences because the vibrational frequencies of the transitions states are the same as for the products. The internal rotations of the two fragments in the transition states are also the same as the product rotations. However, the rotational constant for the overall rotation of the transition state complex at the centrifugal barrier depends on the angular momentum, which is conserved between the energized molecule and the transition state. The treatment of Waage and Rabinovitch [30] for this degree of freedom can be applied to the barrierless ion–induced-dipole potential, as also discussed by Rodgers et al. [31]. Using eq 14 of reference [30] defining the partition function for the overall rotation of the pseudodiatomic transition state complex, $Q_{\text{cent}}^{\ddagger}(T)$, and the ion–induced-dipole potential, $V(r) = -\alpha q^2/(4\pi\varepsilon_0)^2 2r^4$, one obtains the entropy difference for the rotation in eq 8,

$$\Delta\Delta S_{\text{rot}}^{\ddagger}(T) - \Delta\Delta S_{\text{rot}}(T) = R \ln \frac{Q_{\text{cent},2}^{\ddagger}(T)}{Q_{\text{cent},1}^{\ddagger}(T)} = R \ln \frac{m(\text{R}_1\text{OH})m(\text{R}_2\text{O}^-)\alpha(\text{R}_1\text{OH})^{1/2}}{m(\text{R}_2\text{OH})m(\text{R}_1\text{O}^-)\alpha(\text{R}_2\text{OH})^{1/2}} \quad (8)$$

where m is the mass of the corresponding species, α is the polarizability of the neutral product, q is the ion charge, ε_0 is the permittivity of vacuum, and r is the distance between the ion and the neutral fragments. Qualitatively, eq 8 accounts for how the "looseness" of the transition state complex at the centrifugal barrier depends on the strength of the long range potential. The remaining contribution to the entropy is from translational motion. Using the Sackur-Tetrode equation for the translational entropy of an ideal gas [32a],

$$\Delta\Delta S_{\text{tr}}^{\ddagger}(T) = (3/2) R \ln[m(\text{R}_1\text{OH}\cdot\cdot\text{R}_2\text{O}^-)/ m(\text{R}_2\text{OH}\cdot\cdot\text{R}_1\text{O}^-)] = 0 \quad (9a)$$

$$\Delta\Delta S_{\text{tr}}(T) = (3/2) R \ln[m(\text{R}_1\text{OH})m(\text{R}_2\text{O}^-)/ m(\text{R}_2\text{OH})m(\text{R}_1\text{O}^-)] \neq 0. \quad (9b)$$

Combining eqs 8–9 gives the total entropy differences in eq 10,

$$\Delta\Delta S^{\ddagger}(T) - \Delta\Delta S(T) = (1/2) R \ln \frac{m(\text{R}_2\text{OH})m(\text{R}_1\text{O}^-)\alpha(\text{R}_1\text{OH})}{m(\text{R}_1\text{OH})m(\text{R}_2\text{O}^-)\alpha(\text{R}_2\text{OH})} \quad (10)$$

which is independent of temperature but requires that reactants and products are at some equilibrium temperature.

For the proton-bound alkoxide dimers modeled here, the mass ratio in eq 10 is always close to unity, but the polarizabilities depend on the sizes of the alkanols. Using the polarizabilities given in Table 1, the maximum difference is $\Delta\Delta S^{\ddagger}(T) - \Delta\Delta S(T) = 5.7$ J mol^{-1} K^{-1}, for the extreme case of R_1OH= n-heptanol and R_2OH = methanol. Using $\Delta G = \Delta H - T\Delta S$ at room temperature, that yields a Gibbs energy difference $\Delta\Delta G^{\ddagger}(T) - \Delta\Delta G(T) = -1.7$ kJ/mol, given that $\Delta\Delta H^{\ddagger}(T) = \Delta\Delta H(T)$ because there is zero reverse activation energy. Thus, the difference between the activation entropy and the dissociation entropy is nonzero, but could be corrected using eq 10 for barrierless dissociations on the ion–induced-dipole potential. For systems with reverse activation barriers, where a tight transition state would be appropriate, the vibrational and rotational contributions to $\Delta\Delta S(T)$ and $\Delta\Delta S^{\ddagger}(T)$ would need to be considered explicitly. This issue of the difference between $\Delta\Delta S(T)$ and $\Delta\Delta S^{\ddagger}(T)$ is independent, however, from the issue of the relationship between the apparent entropy actually measured in kinetic method experiments, $\Delta\Delta S_{\text{app}}$, and the thermodynamic entropy of activation, $\Delta\Delta S^{\ddagger}(T)$. The latter more fundamental issue is investigated in this work.

Table 1. Gas-phase acidities and polarizabilities of model alkanols

Acid		$\Delta_{acid}H_{298K}$[a]/kJ mol^{-1}	$\Delta_{acid}H_{0K}$[b]/kJ mol^{-1}	$\alpha/4\pi\varepsilon_0 \times 10^{-24}$ cm^3
MeOH	CH_3OH	1592	1586.7	3.29[c]
EtOH	CH_3CH_2OH	1579	1573.9	5.41[c]
nPrOH	$CH_3(CH_2)_2OH$	1573	1567.8	6.74[c]
nBuOH	$CH_3(CH_2)_3OH$	1571	1565.5	8.9[c]
iBuOH	$(CH_3)_2CH_2CH_2OH$	1568	1562.8	8.9[d]
tBuOH	$(CH_3)_3COH$	1567	1562.0	8.9[d]
sBuOH	$CH_3CHOHCH_2CH_3$	1565	1559.8	8.9[d]
nPnOH	$CH_3(CH_2)_4OH$	1565	1559.9	10.2[d]
nHxOH	$CH_3(CH_2)_5OH$	1565	1559.9	11.5[d]
nHpOH	$CH_3(CH_2)_6OH$	1567	1561.9	12.8[d]

[a]Experimental, Reference [45].
[b]Thermal correction to 0 K using ab initio molecular constants.
[c]Experimental, Reference [44].
[d]Estimated (see text).

Classical RRK Microcanonical Formulation

As described in previous work [10], an approximate analytical estimate of the effective temperature can be derived using the simple classical RRK model for the unimolecular dissociation rates. The classical RRK expression for the microcanonical dissociation rate for product channel j and internal energy E is given by eq 11 [28, 29, 33],

$$k_j^{\mathrm{RRK}}(E) = \nu\left(\frac{E - \Delta_j E_0}{E}\right)^{s-1} \tag{11}$$

where s identical harmonic oscillators of frequency ν comprise the dissociating molecule and $\Delta_j E_0$ is the energy barrier for dissociation. The RRK model can be used to derive a relationship between the effective temperature and the internal energy, E_d, of the dissociating cluster ion [7, 10], eq 12,

$$T_{\mathrm{eff}} \approx \frac{E_d - \Delta_{\mathrm{avg}}E}{R(s-1)} \text{ for } E_d - \Delta_{\mathrm{avg}}E \gg \Delta\Delta E \tag{12}$$

where $\Delta_{\mathrm{avg}}E = (\Delta_1 E + \Delta_2 E)/2$ is the average dissociation energy of the cluster ion. In words, eq 12 says that the effective temperature is proportional to the excess internal energy per degree of freedom, as stated by Beauchamp and co-workers [7]. My previous work [10] further derived an approximation for E_d for the case of metastable ion dissociation in the limit of high ion source temperature, yielding the approximate expression 13 for the effective temperature,

$$T_{\mathrm{eff}} \approx \frac{\Delta_{\mathrm{avg}}E}{R(s-1)[(2\nu\tau)^{1/(s-1)} - 1]} \tag{13}$$

where τ is the characteristic instrumental time window (time-of-flight between the ion source and the field-free region where dissociation occurs). The effective temperature has been conventionally defined as the characteristic temperature of a Boltzmann distribution of the energized molecules that would fragment to give the same product ratio as observed in the experiment [4]. Eq 13 shows that the effective temperature is not a thermodynamic quantity, but rather depends explicitly on molecular and instrumental parameters—namely, the well depth, the size of the ion, the pre-exponential frequency factor, and the instrumental time window. Similar conclusions have been drawn from other theoretical treatments of the kinetic method [6–9, 11]. Detailed numerical simulations [10] verified eq 13 (as an approximation for the RRK model) for high ion source temperatures, and also showed significant curvature in kinetic method plots for species with shallow well depths or small sizes. However, because the classical RRK model is inadequate for calculating quantitative dissociation rates, the extent to which these conclusions apply to real systems may be questionable. Laskin and Futrell [9] have suggested that the curvature in kinetic method plots is strongly overestimated by RRK calculations.

Microcanonical RRKM Kinetic Model

This section describes the statistical rate theory for obtaining microcanonical rate coefficients and outlines the calculation of ion intensities and kinetic method calibration plots using a kinetics model appropriate for competitive dissociation in a tandem mass spectrometer. The molecular parameters of the model alkoxide dimer anions are presented. The model is briefly compared with previous theoretical simulations of the kinetic method [6–11] and the limitations of the present model are addressed.

RRKM Theory

The microcanonical RRKM theory and kinetic model used here is a more rigorous extension of my previous model using the classical RRK theory [10]. Once an ion leaves the ion source of a mass spectrometer or under-

goes its last collision, it is isolated and its total internal energy, E, and angular momentum, J, are constant. The decomposition is therefore properly described by the microcanonical rate coefficient, $k(E,J)$, rather than by the canonical rate coefficient, $k(T)$. The RRKM theory expression for the microcanonical rate coefficient for dissociation to channel j is given by eq 14 [27, 28, 33, 34],

$$k_j(E, J) = \frac{sW_j^{\ddagger}(E - E_R^{\ddagger}(J) - \Delta_j E_0)}{h\rho_j(E - E_R(J))} \quad (14)$$

where s is the reaction degeneracy, $W^{\ddagger}(E)$ is the sum of states of the transition state, $\rho(E)$ is the density of states of the energized cluster ion, and $E_R(J) = hcBJ(J + 1)$ and $E_R^{\ddagger}(J) = hcB^{\ddagger} J(J + 1)$ are the rotational energies of the two-dimensional external rotation of the energized cluster ion and the transition state, respectively. The RRKM rate coefficient in eq 14 depends only on total energy and on the angular momentum J for the two-dimensional external rotation of the cluster ion with energy $E_R(J)$ and degeneracy $g_J = 2J + 1$. This form of RRKM theory accounts for the rotational energy that is excluded from promotion of the dissociation process because of the conservation of total angular momentum, but it does not strictly conserve angular momentum between reactants and products at the state-to-state level [27, 34]. The RRKM calculations are carried out as described previously for analysis of competitive threshold collision-induced dissociation experiments [31, 33, 35]. The details of the treatment of rotational degrees of freedom in the RRKM model are described by Rodgers, Ervin, and Armentrout [31], and the statistical treatment of competitive dissociation channels is described by Rodgers and Armentrout [35] and DeTuri and Ervin [36]. The calculations are performed using a Fortran program, KMODEL, with RRKM code adapted from the CRUNCH data analysis program [37].

A loose transition state model is appropriate for barrierless dissociations of ion–molecule complexes with no reverse activation energies, as assumed for the model systems. The RRKM calculations here employ loose transition states that are variationally located at the top of the centrifugal barrier on the ion-induced dipole potential [31]. The position of the centrifugal barrier determines the pseudodiatomic rotational constant $B^{\ddagger}$. The vibrational frequencies and internal rotational constants of the transition state are equal to those of the two product fragments. The sum and density of states are calculated from harmonic oscillator frequencies and rigid-rotor rotational constants using the Beyer-Swinehart Stein-Rabinovitch direct count algorithm [38–40].

Ion Dissociation Kinetics

In a metastable ion dissociation experiment in a tandem mass spectrometer, the product ion is detected if the metastable cluster dissociates after the flight time t_1 from the ion source through the first mass-selection region to the entrance of the field-free region but before time t_2, the flight time from the source to the exit of the field-free region (entrance to the second mass analyzer). Eqs 1 and 2 represent the elementary reaction steps for the mechanism of irreversible dissociation from the reactant ion cluster into two parallel product channels. The differential rate laws are given by eq 15 [29],

$$\frac{dI_0(t)}{dt} = -[k_1(E, J) + k_2(E, J)]I_0(t) \quad (15a)$$

$$\frac{dI_j(t)}{dt} = k_j(E, J)I_j(t) \quad (15b)$$

where $I_0(t)$ is the parent ion intensity as a function of the time after it leaves the ion source and $I_j(t)$ is the intensity of product ion j. Upon integration of the rate laws from t_1 to t_2, with initial condition $I_j(t_1) = 0$ because product ions formed before the field free region are eliminated in the first mass spectrometer, one obtains the probability of dissociation to the R_jO^- product ion, $D_j(E,J)$, given by eq 16 [6, 10],

$$D_j(E, J) = \frac{k_j(E, J)}{k_{tot}(E, J)}[e^{-k_{tot}(E,J)t_1} - e^{-k_{tot}(E,J)t_2}] \quad (16)$$

where $k_{tot}(E,J) = k_1(E,J) + k_2(E,J)$ and $I_j(E,J)$. The total intensity, I_j, observed at the detector for ion R_jO^- is the probability in eq 16 integrated over the internal energy and angular momentum distribution, $P_0(E,J)$, of the ions coming from the ion source, eq 17,

$$I_j = I_0(0)\int_{E=\Delta_j E_0}^{E=\infty}\left[\sum_{J=0}^{J=J_{max}} P_0(E, J)\, D_j(E, J)\right]dE \quad (17)$$

where $I_0(0)$ is the parent ion source intensity at time $t = 0$ and J_{max} is the maximum J that is energetically accessible at total internal energy E, i.e., where $E = E_R = hcBJ_{max}(J_{max} + 1)$. The distribution $P_0(E,J)$ is determined by the characteristics of the ion source. Here a Boltzmann distribution is used, for which the probabilities of internal energies and angular momenta of the ions sampled from the ion source at temperature T_s are given by eq 18.

$$P_0(E, J)dE = \frac{g_J\rho_{vr}(E - E_R(J))e^{-E/k_BT_s}dE}{\int_{E=0}^{E=\infty}\sum_{J=0}^{J=J_{max}} g_J\rho_{vr}(E - E_R(J))e^{-E/k_BT_s}dE} \quad (18)$$

The denominator of eq 18 is the rotational-vibrational

partition function of the cluster ion at the source temperature, $Q_0(T_s)$. As discussed previously [10], the shape of the internal energy distribution does not greatly affect the metastable ion kinetics as long as the distribution is broad and some ions are hot enough to dissociate during the experimental time window. Regardless of the parent ion distribution, a narrow slice of internal energies is kinetically selected by the dissociation probability given by the exponential terms in eq 16.

Combining eqs 16–18 yields the full expression for the ion intensity of product channel j in eq 19.

$$I_j = \frac{I_0(0)}{Q_0(T_s)} \int_{E=\Delta_j E_0}^{E=\infty} \left[\sum_{J=0}^{J_{max}} g_J \rho_{vr}(E, J) e^{-E/k_B T_s} \cdot \frac{k_j(E, J)}{k_{tot}(E, J)} \left[e^{-k_{tot}(E,J)t_1} - e^{-k_{tot}(E,J)t_2} \right] \right] dE \qquad (19)$$

The product ion intensities I_1 and I_2 are calculated by numerical integration of eq 19. Kinetic method plots are then simulated by plotting $\ln(I_2/I_1)$ versus $\Delta\Delta H \approx \Delta\Delta E_0 = \Delta_2 E_0 - \Delta_1 E_0$. The dependence of the intensity ratio on $\Delta\Delta E_0$ is implicit in the calculation of the RRKM rate coefficients, $k_j(E)$, which depend on $\Delta_j E_0$. According to eq 7, the effective temperature is calculated by equating the slope of $\ln(I_2/I_1)$ versus $\Delta\Delta H$ with $(-1/RT_{eff})$, or for individual measurements $T_{eff} = -\Delta\Delta H/R \ln(I_2/I_1)$ assuming $\Delta\Delta S_{app} \approx 0$.

Internal Energy

The time window of the experiment kinetically selects a subset of the metastable ions in the parent distribution that have the correct amount of internal energy to dissociate in the field free region of the mass spectrometer. The mean internal energy of ions that undergo dissociation to either channel within the experimental time window is given by eq 20,

$$\langle E_d \rangle = \frac{\int_{E=0}^{E=\infty} E P_0(E)[D_1(E) + D_2(E)]dE}{\int_{E=0}^{E=\infty} P_0(E)[D_1(E) + D_2(E)]dE} \qquad (20)$$

where the sums over rotational states have been suppressed for notational convenience. The value of $\langle E_d \rangle$ is always greater than the lowest dissociation energy, $\Delta_j E_0$. Eq 20 gives the joint average for both dissociation channels—actually the ions dissociating into the two channels have somewhat different energy distributions for $\Delta\Delta E \neq 0$. Laskin and Futrell [9] characterize the two distributions by different transition state temperatures in the finite heat bath formalism. This effect gives rise to the curvature in kinetic method plots.

Model Systems

The chosen model systems are alkyl alcohols ranging in size from methanol to heptanol with various alkyl group structures. Geometries are obtained at the HF/6-31G* level using Gaussian [41]. Because the present goal is merely to obtain physically reasonable parameters for model calculations, a single conformation has been chosen for each species. For the n-alkanols and n-alkoxides, stretched conformations are used (neglecting intramolecular interactions between the alkyl chain and the oxygen so that the reverse activation energies due to those interactions in the actual alkanols [42] are excluded in the model). Vibrational frequencies are calculated at the HF/6-31G* level and are scaled by a factor of 0.89 [43]. For the rotational constant of the two-dimensional external rotations, the geometric mean is taken of the two most similar rotational constants, i.e., $B \approx (BC)^{1/2}$ or $(AB)^{1/2}$. The reaction degeneracies are unity ($s = 1$) for all systems described here except those with methoxide (CH_3O^-) or *tert*-butoxide [$(CH_3)_3CO^-$] as a product, for which $s = \sigma/\sigma^{\ddagger} = 1/3$ to account for rotational symmetries (119) that are not included in the sums and densities of states [27, 36]. The polarizabilities of the alkanol products (Table 1), required for calculation of the position of the centrifugal barrier on the ion–induced- dipole potential, are taken from experiments where available [44]. For larger alkanols, the polarizabilities are estimated from the values of smaller alkanols with $\alpha/4\pi\varepsilon_0 = 1.3 \times 10^{-24}$ cm^3 added per CH_2 group. Experimental gas phase acidities [45], $\Delta_{acid}H_{298}$, are listed in Table 1 and are corrected there to 0 K using the calculated molecular parameters. These are taken as the true values in the simulations. Table 1 gives abbreviations for the alkanol species.

Relationship to Previous Work

Brauman and co-workers [8] reported the first full RRKM theory treatment of the kinetic method. The primary difference between their model and the present simulation is that they ignored the exponential kinetic terms in eq 16 (effectively using $t_1 = 0$ and $t_2 = \infty$) and instead replaced $P_0(E)$ with a displaced Boltzmann distribution (internal energies shifted up by an arbitrary amount) as an ad hoc method of selecting the internal energy distribution for the dissociating ions. The present work, as well as two previous simulations using classical RRK theory by Bojesen and Breindahl [6] and by Ervin [10] and the RRKM treatment by Drahos and Vékey [11, 12], properly uses the kinetic expression in eq 16 to select the energy distribution that would be observed in an experiment. In the RRKM and finite heat bath theory treatments of Laskin and Futrell [9], the integration over the distribution of the internal energies of the dissociating ions represented by eq 17 is replaced by evaluation at the single most-probable value of the internal energy. Laskin and Futrell [9] used a fixed transition state model. The loose, variational transition

state at the centrifugal barrier used here is appropriate for electrostatically or hydrogen-bound complexes with a barrierless dissociation potential. The present work and Brauman's study [8] treat angular momentum effects in a fairly rigorous manner, while the other treatments cited above are apparently for zero angular momentum.

Bojeson and Breindahl [6] modeled proton-bound amine dimers, and investigated the effect of variation of the RRK model parameters in eq 11 on effective temperature and internal energy distributions. Brauman and co-workers [8] systematically varied the average dissociation energy and the size of the cluster ion for fixed internal energy distributions. Drahos and Vékey [11] randomly varied the time window (t_1, t_2) and the source temperature for a single propylamine/butylamine proton-bound dimer. Laskin and Futrell [9] varied the number of vibrational degrees of freedom of model peptide clusters, changed the frequencies in the transition states to vary the entropy of activation, and used three time windows. In this work, the effect of various molecular and instrumental parameters are considered systematically for systems with no entropy effects, and kinetic method plots for realistic sets of molecular species with entropy differences are simulated.

Limitations of the Present Model

The present treatment is subject to the approximations of RRKM theory, but this form of statistical unimolecular rate theory has proven accurate in many studies of ion dissociation processes [28]. The present kinetics model applies strictly to metastable ion dissociation experiments. Collision-induced dissociation experiments differ in two ways: The initial internal energy distribution of the cluster ion is determined by the collision conditions and the time window is from $t_1 = 0$ at the moment of the collision to t_2 when the ions enter the mass spectrometer detector. Both effects tend to create a broader and higher internal energy distribution of dissociating ions than in metastable ion dissociation, but the distribution is still non-Boltzmann. The quantitative results of the simulations reported here may be influenced by the size, well-depth, and frequency distributions of the alkoxide/alkanol model systems, chosen because of our studies of these systems [36, 46] and past applications of the kinetic method to similar systems [2, 14, 47–49]. The ab initio calculations provide a physically realistic, self-consistent set of frequencies across the series of alcohols, but the use of a single conformation and the harmonic oscillator approximation for vibrations neglects anharmonicity effects on the density of states in real systems. Although some of the low-frequency vibrational modes would be better treated as free or hindered rotors, the vibrational sums and densities of states largely cancel in the RRKM calculations and more sophisticated treatments or a higher level of ab initio theory are unnecessary for model calculations.

Table 2. Baseline parameters for model calculations

$t_1 = 2 \times 10^{-5}$ s
$t_2 = 4 \times 10^{-5}$ s
$T_s = 1000$ K
$\Delta_{avg}E_0 = (\Delta_2E_0 + \Delta_1E_0)/2 = 115$ kJ/mol
$\Delta\Delta E_0 = \Delta_2E_0 - \Delta_1E_0 = 0$

Symmetric Cluster Ions

This section investigates the behavior of kinetic method plots for symmetric ion clusters, $R_1OH = R_2OH$, which can only be studied theoretically. For symmetric dissociation reactions, the entropy term is identically zero, $\Delta\Delta S = \Delta\Delta S^{\ddagger} = 0$, while $\Delta\Delta E$ can be varied artificially. Also, for symmetric systems $\Delta\Delta E = \Delta\Delta H = \Delta\Delta G$ at all temperatures, bypassing questions about the use of enthalpies versus Gibbs energies in the kinetic method. The behavior of the $\ln(I_2/I_1)$ versus $\Delta\Delta H$ curves is considered for variation of the ion source temperature, the well-depth, size, vibrational frequencies, molecular structure, and the instrumental time window in Figures 2 to 7, respectively. For the simulations, the parameters in Table 2 are chosen as typical values for a metastable ion dissociation experiment. These apply to all simulations except as noted. The well-depth of $\Delta_{avg}E = 115$ kJ/mol is used as a typical value based on complexation energies of proton-bound alkoxide dimers found in the NIST ion thermochemistry database [50]. In Figures 2 to 7, $\Delta\Delta E$ is varied over the range ± 15 kJ mol^{-1} and ion intensity ratios of approximately 1000:1 to 1:1000 are plotted. The condition $\Delta\Delta S = 0$ for the symmetric cluster ions ensures that the plots of $\ln(I_2/I_1)$ versus $\Delta\Delta E$ are exactly symmetric with respect to inversion about the origin, where $\Delta\Delta E = 0$ and $\ln(I_2/I_1) = 0$. The figures also show T_{eff} and $\langle E_d \rangle$ calculated for $\Delta\Delta E = 0$.

Source Temperature Dependence

Figure 2 shows the dependence of the kinetic method plots and effective temperatures on ion source temperatures for tert-butoxide/tert-butanol clusters. Eq 13 indicates that the effective temperature is independent of the actual ion source temperature, but that applies only in the high-temperature limit, as discussed previously [9–11]. If T_s is smaller than the effective temperature in the high-temperature limit, then the slopes of the kinetic plots will instead be determined by the source temperature ($T_{eff} = T_s$) and not the parameters given by eq 13 [10]. As expected, the effective temperatures in Figure 2b are relatively insensitive to the source temperature for high parent ion temperatures, but are limited by the source temperature at low T_s. For ion source temperatures below room temperature, the parent cluster ions are stable and the number of dissociation products would actually be undetectably small

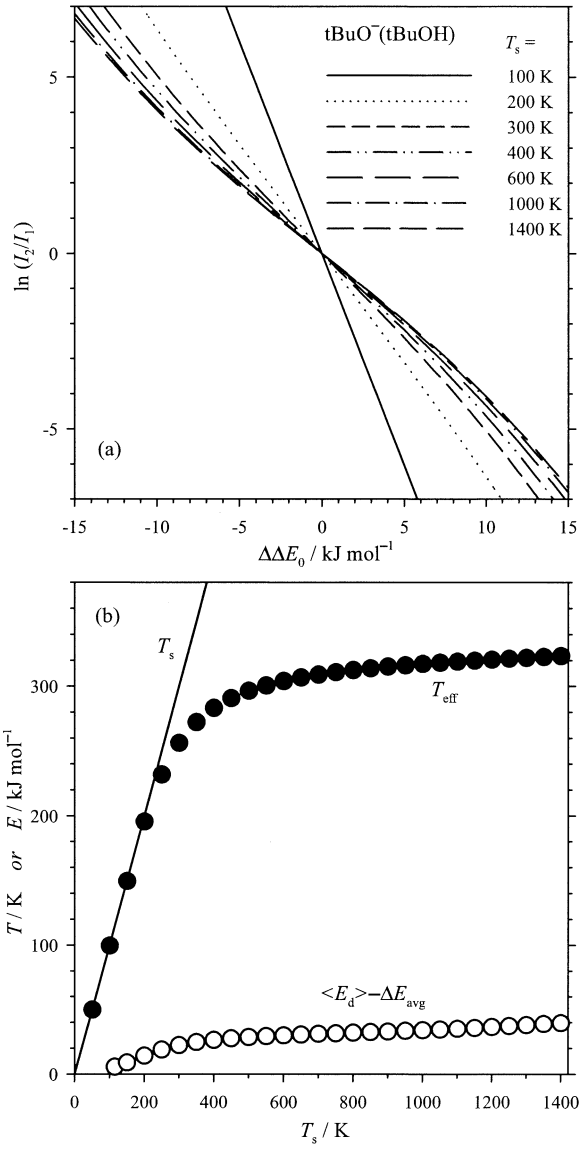

Figure 2. (**a**) Numerical simulation of the kinetic method for model t-butoxide/t-butanol complexes at various ion source temperatures with other parameters given in Table 2. (**b**) The dependence of the effective temperature T_{eff} and the mean excess internal energy $\langle E_d \rangle$ on ion source temperature T_s. Numerical simulations (points); upper limit of $T_{eff} = T_s$ (line).

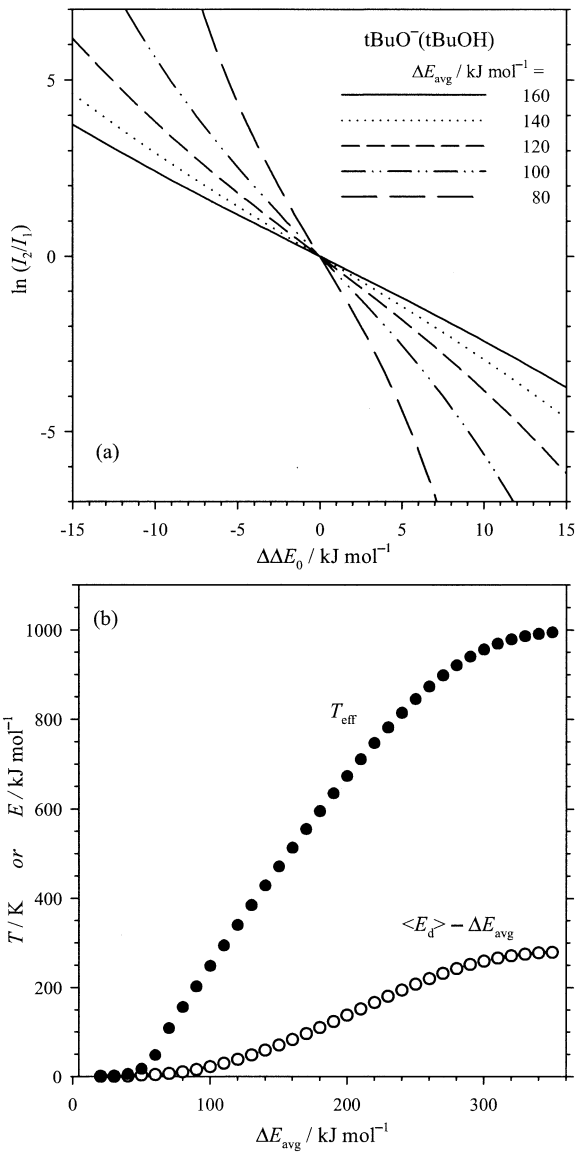

Figure 3. (**a**) Numerical simulation of the kinetic method for model t-butoxide/t-butanol complexes at various well-depths ΔE_{avg} of the cluster ion with other parameters given in Table 2. (**b**) Dependence of the effective temperature and mean excess internal energy on the well-depth.

for a 10^{-5} s time window. For most subsequent simulations presented here, a source temperature of 1000 K is chosen to ensure that the high-temperature limit is maintained while other parameters are varied over reasonable ranges.

Well-Depth Dependence

To investigate the dependence of the kinetic method correlations on the depth of the well of the ion–molecule complex, $\Delta_{avg}E$ is artificially varied for the symmetric tert-butoxide/tert-butanol complex. The kinetic plots are shown in Figure 3a. The cluster ions with shallower wells show both smaller effective temperatures (steeper negative slopes) and greater curvature. The effective temperatures are plotted versus $\Delta_{avg}E$ in Figure 3b. Over a broad range of $\Delta_{avg}E$ (from 60 to 240 kJ/mol for this system), the effective temperature varies linearly with the well depth as suggested by eq 13 although the intercept is not zero. For deeper wells, which would represent covalently bound complexes, the effective temperature stops increasing simply because it cannot exceed the ion source temperature as discussed above. For very shallow wells, the effective temperature goes to zero (infinite slope). This region corresponds to rapidly dissociating systems where most parent ions dissociate before reaching the field free region.

Although a series of cluster ions with the same type

of ion–molecule interaction (e.g., hydrogen bonding for the alkoxide/alkanol complexes) are likely to have similar well depths, a variation of 10 to 15% is common. According to the NIST ion thermochemistry database [50], experimental complexation energies for various alkoxide/alkanol complexes range from 107 to 121 kJ/mol. Based on the data in Figure 3b, that would yield effective temperatures ranging from 281 K to 344 K or up to a 20% variation of individual T_{eff} values. For $\Delta\Delta E \approx 10$ kJ/mol, that would yield a variation of up to 2 kJ/mol from the expected values of $\Delta\Delta E$ for complexes with different well depths. However, this variation is not random because both the well depths and the acidities may be correlated with the sizes of the alkanols.

Size Dependence

Figure 4a presents simulated kinetic method plots for symmetric RO^-(ROH) complexes with various alkyl chain lengths. The variation in slopes shows the strong dependence of the effective temperature on the size of the cluster ion. Figure 4b shows the dependence of the effective temperature on the number of vibrational degrees of freedom of the cluster ion. As approximated by eq 13, T_{eff} is proportional to $\Delta_{avg}E/R(s - 1)$, the average dissociation energy per degree of freedom at the threshold energy, and is inversely proportional to $[(2\nu\tau)^{1/(s-1)} - 1]$, which expresses the dependence of the kinetic selection of the energies of the dissociating ions on the characteristic frequency factor, time window, and number of vibrational oscillators [10]. The size dependence due to the $1/[(2\nu\tau)^{1/(s-1)} - 1]$ factor is more important than the $\Delta_{avg}E/R(s - 1)$ factor, and therefore effective temperature increases with size—larger cluster ions dissociate more slowly so a higher internal energy is required for dissociation within a fixed experimental time window. However, eq 13 cannot quantitatively reproduce the effective temperature unless ν and s are empirically adjusted. This is due to the quantitative limitations of the classical RRK model.

The size dependence of the effective temperature is dramatic, from $T_{eff} = 24$ K for MeO^-(MeOH) to $T_{eff} = 394$ K for $nHpO^-$(nHpOH). Dimer anions the size of the MeO^-(MeOH) and EtO^-(EtOH) probably dissociate too rapidly for practical metastable ion dissociation measurements, but cluster ions the size of the propoxide/propanol dimer ($T_{eff} = 62$ K) or propoxide/ethanol have been used experimentally in kinetic method calibrations along with larger species [14, 47, 49]. Laskin and Futrell [9] investigated much larger species, up to 500 degrees of freedom, and their work shows that the effective temperatures plateau for very large species, which act as their own thermal heat bath.

Vibrational Frequency Dependence

Figure 5 shows kinetic plots where the frequencies of all vibrational modes in the cluster ions and transition states have been scaled by 70 to 130% from the original values. As predicted by eq 13, lower frequencies (ν) produce higher effective temperatures. Species with lower frequencies have higher densities of state. This affects the density of states of the energized molecule (denominator of eq 14) more than the sum of states of the transition state (numerator) because of the higher internal energy of the energized molecule. Therefore, the cluster ions with lower frequencies have slower dissociation rates, requiring a higher effective temperature or internal energy to dissociate within the experimental time window. However, the effect of vibrational frequencies on the effective temperatures is not as strong as that of size, for physically reasonable varia-

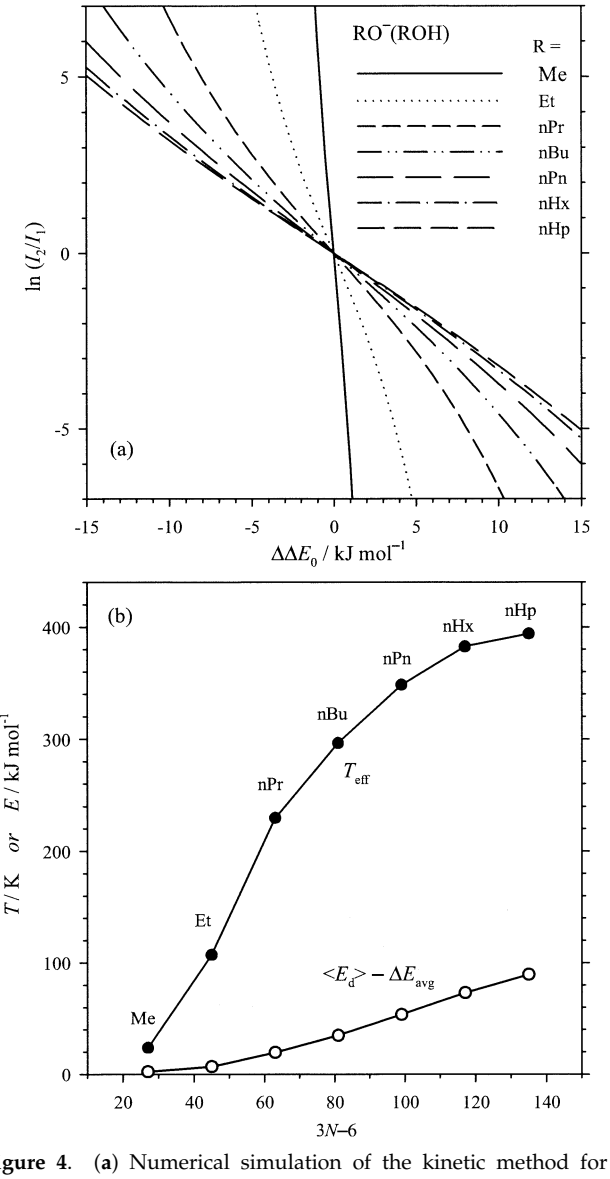

Figure 4. (**a**) Numerical simulation of the kinetic method for various symmetric alkoxide/alkanol complexes of different sizes with other parameters as given in Table 2. (**b**) Dependence of the effective temperature and the mean excess internal energy on the well-depth on the number of vibrational degrees of freedom of the cluster ion, $3N-6$, where N is the number of atoms.

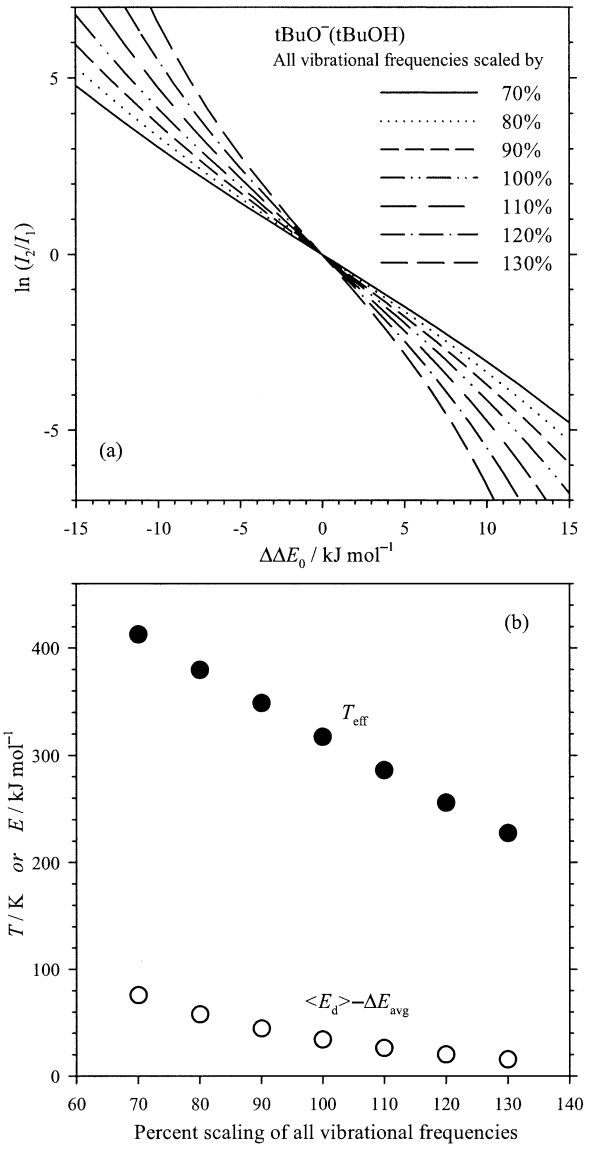

Figure 5. (**a**) Numerical simulation of he kinetic method for model t-butoxide/t-butanol complexes with vibrational frequencies of all modes in the cluster ion and transition states scaled by the given percentages, with other parameters as given in Table 2. (**b**) Dependence of the effective temperature and mean excess internal energy on the percentage scaling of vibrational frequencies.

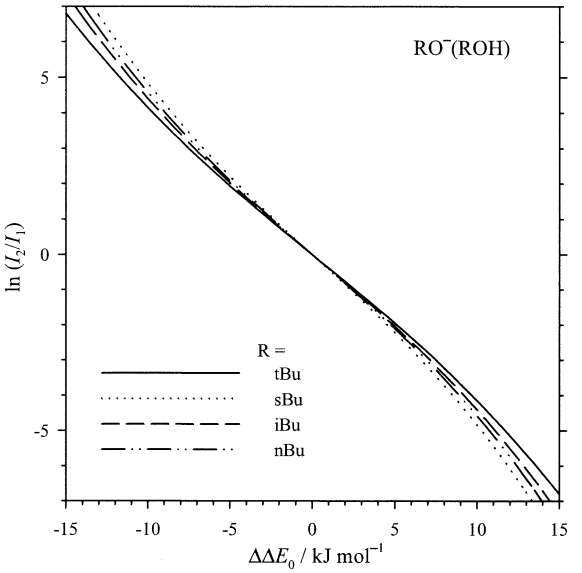

Figure 6. Numerical simulation of the kinetic method for symmetric butoxide/butanol complexes with different butyl group structures: tert-butyl (tBu), 2-butyl (sBu), iso-butyl (iBu), and n-butyl (nBu). Other parameters are given in Table 2.

tions. Anharmonicity effects tend to mimic lower frequencies [51].

Structure Dependence

Molecular structure effects can be probed by examining a series of symmetric alkanol–alkoxide complexes of the same size but different alkyl group structures. Figure 6 presents simulated kinetic method correlation plots for $RO^-(ROH)$ cluster ions where R = tert-butyl, iso-butyl, sec-butyl, and n-butyl. It is apparent that the effective temperatures are quite similar for all four alkyl structures, with some deviations in curvature at the largest $\Delta\Delta E$ values. In the present simulation, the only differences among these butoxide and butanol species are the distribution of vibrational frequencies and the rotational constants. The system parameters in Figure 6 are chosen to give no variation in T_{eff} due to size and well depth, but nevertheless the different curvature for the various species would yield variation of up to 15% in $\Delta\Delta E$, as quantified by the horizontal spread of the curves for a given value of $\ln(I_2/I_1)$. For the acidity differences of 2–6 kJ/mol between the isomeric butanols (Table 1), this represents an absolute deviation of up to 0.3–0.9 kJ/mol. Use of different conformational structures for the alkanols would have a similar effect as the structural isomers in Figure 6, but the anharmonicity effects on the densities of states from dynamic exchange between conformations would need to be considered separately.

Time Window Dependence

Eq 13 also predicts a dependence of the effective temperatures on the instrumental time window. Figure 7 shows simulated kinetic method plots and effective temperatures for a range of time windows, with the arbitrary constraint $t_2 = 2t_1$. The effective temperatures decrease for longer (later) time windows. Early time windows select higher-energy ions from the internal energy distribution from the source, while late time windows select ions with internal energies nearer threshold. The time window is usually the same for a given instrument or set of experiments, and thus is not usually a variable parameter. Qualitatively, mass spectrometers with shorter time windows such as time-of-flight or high-voltage sector instruments will exhibit

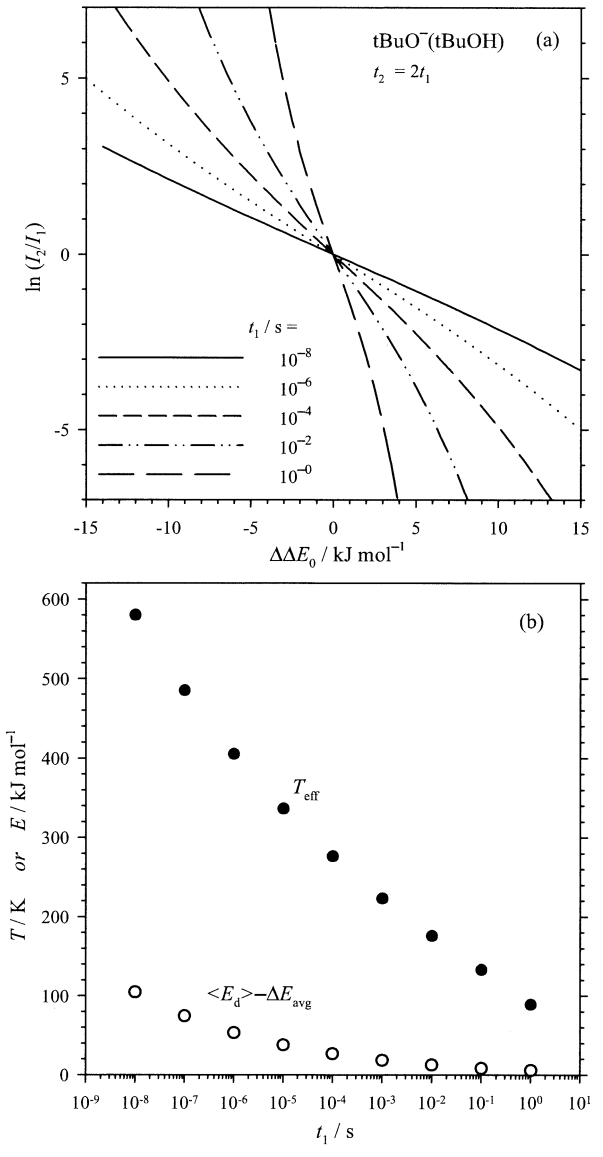

Figure 7. (**a**) Numerical simulation of the kinetic method for various time windows with $t_2 = 2t_1$ and other parameters as given in Table 2. (**b**) Dependence of the effective temperature and the mean excess internal energy on t_1.

higher effective temperatures than those with longer time windows such as triple quadrupoles or ICRs.

Curvature of Kinetic Method Plots

Some of the kinetic plots in Figures 2 to 7 exhibit significant curvature. The curvature is most pronounced for rapidly dissociating ions, including cluster ions with shallow wells or small sizes, and experiments with long time windows, as previously predicted by the RRK model calculations [10]. The curvature is less important for the largest cluster ions and for small values of $\Delta\Delta E$. Contrary to the suggestion of Laskin and Futrell [9], the curvature is not an artifact of the level of the rate calculation (RRK versus RRKM) or the sophistication of the determination of the density of states, but rather the curvature results from the intrinsic kinetic behavior of the rapidly dissociating small systems. The form of the statistical rate theory will affect curvature only to the extent that the magnitudes of the predicted rate constants are different. Laskin and Futrell [9] modeled large peptide ions for which the curvature is not expected to be as large.

Effective Temperature versus Internal Energy

As shown by eq 13 and Figures 2–7, the value of the effective temperature depends in a complicated way on molecular and instrumental parameters. It is also related to the internal energy of the dissociating ions, as discussed previously [4, 6–11]. In the classical RRK approximation, eq 12 indicates that T_{eff} is proportional to the excess internal energy (energy above the average dissociation energy) per vibrational degree for freedom. For comparison, the average excess internal energies of the dissociating cluster ions, $\langle E_d \rangle$ from eq 20 minus the average dissociation energy ΔE_{avg}, are plotted along with the effective temperatures in Figures 2b to 5b and 7b. (The value of ΔE_{avg} is 115 kJ/mol except in Figure 3b where it is varied.) As expected from eq 12, the general trends of T_{eff} and $\langle E_d \rangle - \Delta E_{avg}$ are the similar in each plot. However, the ratios between the two vary significantly as other kinetic and molecular parameters are changed. Therefore, the approximation of eq 12 from classical RRK theory should only be used qualitatively.

Asymmetric Cluster Ions

To examine the behavior of systems where $\Delta\Delta S \neq 0$ and to simulate more realistic experiments, the dissociation of asymmetric alkoxide/alkanol complexes $R_1O^-(R_2OH)$ are modeled, where R_1 and R_2 are different straight-chain alkyl groups from ethyl to n-heptyl. Figure 8a and Figure 9a show simulated kinetic method plots with $\Delta\Delta E_0$ artificially varied over the range −15 to +15 kJ/mol. The other parameters are as given in Table 2; note that the well depths are all set to the single value of ΔE_{avg} = 115 kJ/mol, eliminating the additional source of variation in T_{eff} from different complexation energies. Because $\Delta\Delta S \neq 0$, the plots no longer pass exactly through the origin. According to eq 7, the y-intercept of these plots is equal to $\Delta\Delta S_{app}/R$ yielding the apparent entropy, designated here as $\Delta\Delta S^{(y)}_{app}$ to denote the apparent entropy obtained from the y-intercept of a simulated kinetic method plot. Because the two product channels in the model alkoxide/alkanol cluster ions nearly meet the isentropic criterion, the deviations of $\Delta\Delta S^{(y)}_{app}$ from zero are small.

Standard Kinetic Method

Figure 8 shows a simulation of a common implementation of the standard form of the kinetic method [4], in which the calibration curve is created from measurements of multiple proton-bound alkoxide dimer pairs. The experimental enthalpies of deprotonation, $\Delta_{acid}H_0$,

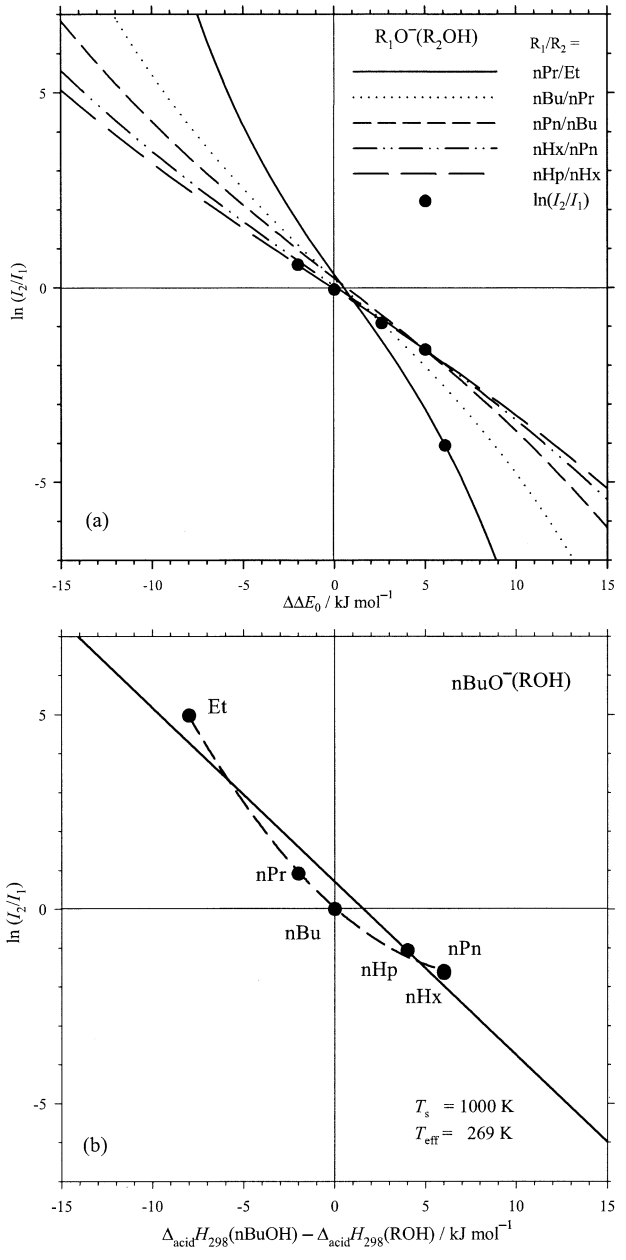

Figure 8. (**a**) Numerical simulation of kinetic method plots for various asymmetric alkoxide/alkanol complex ions. The lines show the simulations and the solid circles show the value that would be obtained for the experimental acidities given in Table 1. (**b**) Simulation of a standard kinetic method calibration plot using the data from part (**a**) as described in the text. The solid line is a linear regression and the dashed line is a quadratic fit.

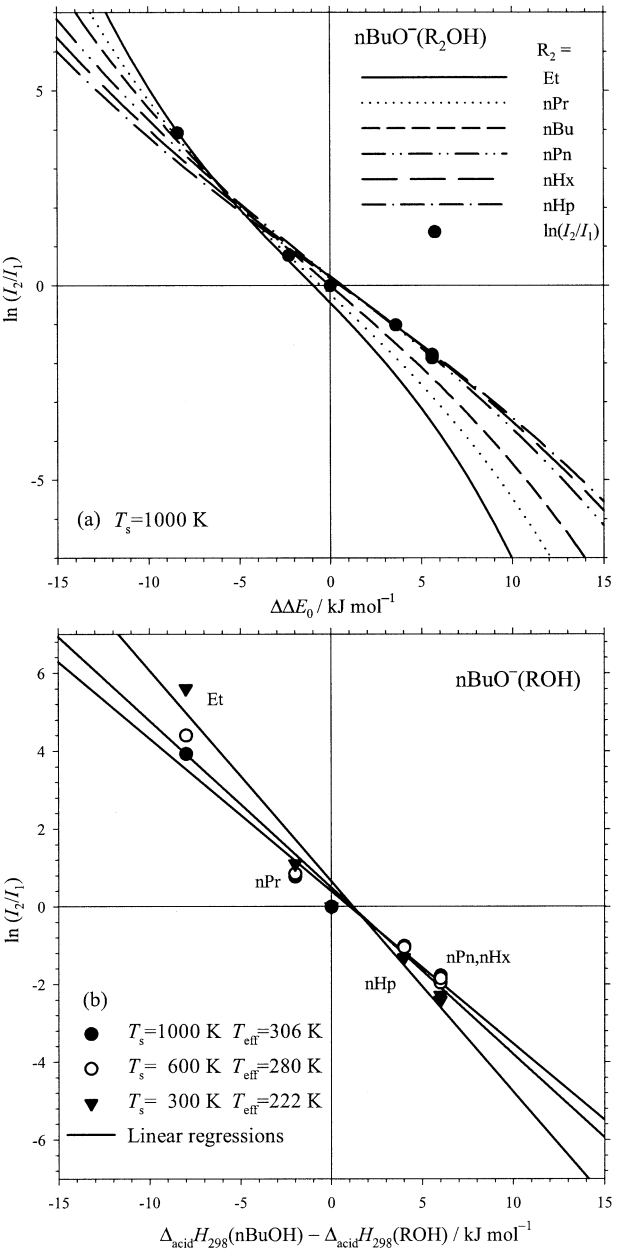

Figure 9. (**a**) Numerical simulation of kinetic method plots for various asymmetric alkoxide/alkanol complex ions. The lines show the simulations and the solid circles show the $\ln(I_2/I_1)$ value that would be obtained for the experimental acidities given in Table 1. (**b**) Simulation of a single-reference isentropic kinetic method calibration plot using the data from part (**a**) for a source temperature of 1000 K, and additional simulations for source temperatures of 300 and 600 K.

compiled in Table 1 are taken as the true values. In Figure 8a, the circles denote the values of $\ln(I_2/I_1)$ that would be observed for the various proton-bound dimers at $\Delta\Delta E_0 = \Delta_{acid}H_0(R_2OH) - \Delta_{acid}H_0(R_1OH)$. The effective temperatures calculated the for individual points are 178 K for R_1/R_2 = n-propyl/ethyl, 263 K for n-butyl/n-propyl, 450 K for n-pentyl/n-butyl, and 411 K for n-heptyl/n-hexyl. The effective temperature for n-hexyl/n-pentyl is nominally 0 K because coincidentally $\Delta\Delta H = 0$ from the experimental data Table 1, but $\ln(I_2/I_1) = 0.05$ from the simulation rather than zero. In Figure 8b, the individual values are all referenced relative to R_2OH = *n*-butanol and plotted against $\Delta\Delta H_{298}$. For example, the ratio I_2/I_1 for $nBuO^-$(EtOH) in Figure 8b is calculated by multiplying the ratios for $nBuO^-$(nPrOH) and $nPrO^-$(EtOH) from Figure 8a. In this format, the individual effective temperatures are 194 K for ethyl/n-butyl, 263 K for n-propyl/n-butyl, 450 K for n-pentyl/n-butyl, 436 K for n-hexyl/n-butyl, and

451 K for n-heptyl/n-butyl. The linear regression of the points in Figure 8b yields an average effective temperature of 269 K for the overall calibration. The effective temperatures for individual proton-bound dimers thus differ by −28% to +68% from the average. Figure 8b shows that the calibration curve does not pass through the origin as assumed in the standard kinetic method. The horizontal distances of the points from the calibration line represent the errors that would occur for hypothetical unknowns identical to the corresponding species, −1.6 kJ/mol for ethanol, +1.5 kJ/mol for n-propanol, +1.6 kJ/mol for n-butanol, −0.8 kJ/mol for n-pentanol, −0.7 for n-hexanol, and $+0.0_2$ kJ/mol for n-heptanol. The distribution of these errors may be described statistically by the standard deviation, $s = 1.3$ kJ/mol, or the 90% confidence interval, $t_{90}s = \pm 2.8$ kJ/mol. *However*, these are systematic errors and not random errors that could be reduced by replicate measurements—in particular, there is no expectation that a new unknown should fall randomly within the same distribution of deviations. Indeed, based on the trends one could safely predict that methanol would have a larger error than n-octanol (the smaller species would exhibit a low T_{eff} and high curvature in the kinetic plot). Figure 8b also shows a quadratic curve (dashed line); it reproduces the curvature well, but quadratic fits to experimental data might not be justified because of random uncertainty in I_2/I_1 and $\Delta\Delta H$.

Single-Reference Isentropic Kinetic Method

In the single-reference form of the isentropic kinetic method [4, 52], all of the calibration compounds are paired with a single reference compound. In this scheme, one assumes as an approximation that $\Delta\Delta S^{\ddagger}(T)$ is the same for all of the dissociating cluster ions, rather than the more severe assumption of the standard kinetic method that $\Delta\Delta S^{\ddagger}(T) = 0$. Figure 9a shows a simulation where n-butanol is employed as the single reference acid. Figure 9b shows the resulting calibration plot for the $T_s = 1000$ K data in Figure 9a, and in addition shows the calibrations obtained in simulations using ion source temperatures of 300 and 600 K. For the $T_s = 1000$ K simulations, the average effective temperature from the linear regression is 306 K and the effective temperatures of the individual cluster ions range from 20% lower than the average for ethyl/n-butyl to 55 % higher for n-hexyl/n-butyl. The deviations between the $\Delta\Delta H$ values from the calibration plots in Figure 9b and the true values are characterized by $s = 1.0$ kJ/mol ($t_{90}s = \pm 2.1$ kJ/mol) for $T_s = 300$ K, $s = 0.9$ kJ/mol ($t_{90}s = \pm 2.0$ kJ/mol) for $T_s = 600$ K, and $s = 0.8$ kJ/mol ($t_{90}s = \pm 1.8$ kJ/mol) for $T_s = 1000$ K. The errors are slightly larger for the lower source temperatures because the effective temperatures are somewhat lower (compare Figure 2), and therefore the mean internal energies are lower and closer to threshold, resulting in greater curvature in the plots. The slightly larger errors of the standard kinetic method in Figure 8b relative to the single-reference kinetic method in Figure 9b are mainly due to the fact that the chosen calibration species have a more extreme range of cluster ion sizes for the former and therefore a larger range of effective temperatures.

Apparent Entropy

Because the dissociation entropies of the alkoxide/alkanol model systems are fairly well matched (by design), those systems do not show strong entropy effects. For simulation purposes, $\Delta\Delta S^{\ddagger}$ can be varied systematically by scaling the frequencies of one dissociation channel. Figure 10a shows simulated kinetic method plots for tert-butoxide/tert-butanol complexes where the vibrational frequencies for channel 2 have been scaled by 80 to 120% from the original values. The variation of the *y*-intercepts, $\Delta\Delta S^{(y)}_{app}$, is qualitatively consistent with the expected entropy changes. When channel 2 has lower vibrational frequencies and therefore a higher density of states, $\Delta\Delta S^{\ddagger}$ is greater than zero and channel 2 is entropically favored leading to $I_2/I_1 > 1$ when $\Delta\Delta E_0 = 0$.

Figure 10b compares the apparent entropies obtained from the *y*-intercepts, $\Delta\Delta S^{(y)}_{app}$, with thermodynamic entropies of the transition states, $\Delta\Delta S^{\ddagger}(T)$, calculated by statistical mechanics from the ab initio molecular constants (in the harmonic oscillator rigid-rotor approximation, the same as used for calculation of the sums and densities of states in the RRKM model). According to eq 10, $\Delta\Delta S^{\ddagger}(T) = \Delta\Delta S(T)$ for these model systems because the masses and polarizabilities for the two channels are identical. Because the entropies vary with temperature, one must choose a temperature for comparison. Three plots of $\Delta\Delta S^{\ddagger}(T)$ are shown in Figure 10b, calculated for $T = 300$ K, $T = 600$ K, and $T = T_{eff}$. The effective temperatures are calculated from the slopes of the plots in Figure 10a and range from 267 K for the 70 % scaling of vibrational frequencies to 391 K for the 130 % scaling. *None* of these statistical mechanical entropies of activation match the apparent entropy changes taken from the intercepts. Matching the apparent entropies from the intercepts would require temperatures ranging from 115 K for the 70% scaling to 170 K for the 130% scaling, i.e., no single temperature is adequate. The thermodynamic entropies calculated for $T = T_{eff}$ follow the roughly the same trend as the apparent entropies from the simulations, but are a factor of 2.4 to 2.8 times higher for the 70 to 130% vibrational scaling, respectively. Test calculations on clusters of different sizes using the 90% scaling of vibrational frequencies show that the constant of proportionality varies from system to system: $\Delta\Delta S^{\ddagger}(T = T_{eff})/\Delta\Delta S^{(y)}_{app} = 7.1$ for EtOH(EtO^-), 2.4 for nPrOH($nPrO^-$), and 2.1 for nHpOH($nHpO^-$). Thus, the apparent entropy term from the correlation given by eq 7 does not equal the thermodynamic entropy of activation, either at the effective temperature or for any fixed temperature.

If the apparent entropy is not a thermodynamic

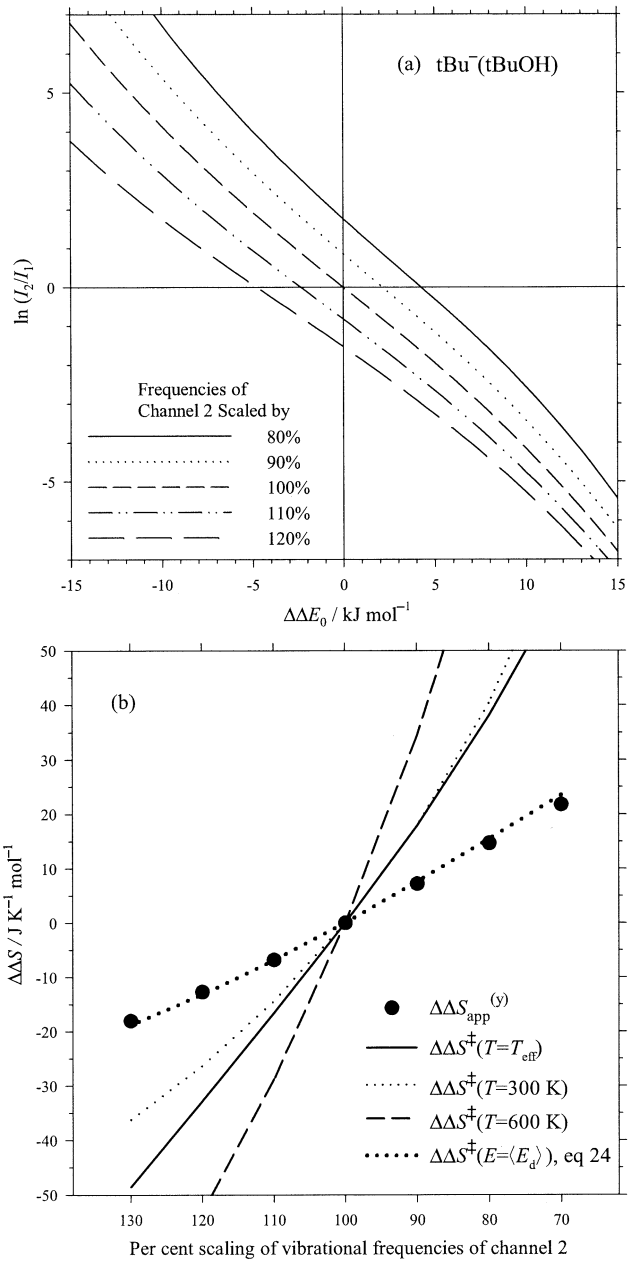

Figure 10. (**a**) Numerical simulation of kinetic method plots for model tert-butoxide/tert-butanol complexes with the vibrational frequencies of the second dissociation channel scaled by various percentage in order to change the entropy difference. (**b**) Dependence of the apparent entropies (solid circles) obtained from the *y*-intercepts in part (**a**). Thermodynamic entropy differences calculated by statistical mechanics at various temperatures, T = 300 K (light dotted line), T = 600 K (dashed line), and at $T = T_{eff}$ (solid line). The heavy dotted line is the microcanonical entropy difference, $\Delta\Delta S^{\ddagger}(\langle E_d \rangle)$, calculated by eq 24.

entropy of activation difference at some defined temperature, then what is it? It certainly is related to the relative entropic factors controlling the kinetic dissociation rates for the two channels, i.e., it is related to the pre-exponential frequency factors. However, under the conditions of metastable ion dissociation in a mass spectrometer, the energy distribution is not characterized by the Boltzmann distribution, as would be appropriate for a macrocanonical ensemble of ions in equilibrium at a temperature T, but instead is closer to a microcanonical ensemble at fixed internal energy. The Boltzmann equation defines the absolute molar entropy of a microcanonical ensemble by eq 21 [32b],

$$S(E) = R \ln W(E) \tag{21}$$

where $W(E)$ is the number of microstates accessible at energy E. For a microcanonical ensemble of dissociating complexes with fixed internal energy E, the entropy term would be given by eq 22,

$$\Delta\Delta S^{\ddagger}(E) = R \ln \frac{W_2^{\ddagger}(E - \Delta_2 E_0)}{W_1^{\ddagger}(E - \Delta_1 E_0)} \tag{22}$$

where $W^{\ddagger}(E)$ is is the statistical sum of states from eq 14. For the metastable ion kinetic method experiment, the number of states should be integrated over the energy distribution of dissociating ions to yield the apparent entropy $\Delta\Delta S_{app}$ in eq 23.

$$\Delta\Delta S_{app} = R \ln \left(\frac{\int_{\Delta_2 E_0}^{\infty} P_0(\varepsilon)\, D_2(\varepsilon) W_2^{\ddagger}(\varepsilon - \Delta_2 E_0) d\varepsilon}{\int_{\Delta_1 E_0}^{\infty} P_0(\varepsilon)\, D_1(\varepsilon) W_1^{\ddagger}(\varepsilon - \Delta_1 E_0) d\varepsilon} \right) \tag{23}$$

Evaluating the sum of states at the mean energy of the dissociating ions from eq 20 gives the approximation of eq 24,

$$\Delta\Delta S_{app} \approx \Delta\Delta S^{\ddagger}(\langle E_d \rangle) = R \ln \frac{W_2^{\ddagger}(\langle E_d \rangle - \Delta_2 E_0)}{W_1^{\ddagger}(\langle E_d \rangle - \Delta_1 E_0)} \tag{24}$$

which dispenses with the integration in eq 23. That approximation is reasonable for metastable ion dissociation because a relatively narrow slice of ion energies is kinetically selected by the experimental time window. Figure 10b shows that $\Delta\Delta S^{\ddagger}(\langle E_d \rangle)$ from eq 24, for which the sums of states are calculated by the Beyer-Swinehart direct count algorithm, nicely matches values of $\Delta\Delta S_{app}^{(y)}$ obtained from the numerical simulations. Thus, the measured apparent entropy $\Delta\Delta S_{app}^{(y)}$ can be identified as the entropy difference of the two channels for a microcanonical ensemble of transition state species specified by the mean internal energy of the dissociating ions. The mean energy of dissociating ions, $\langle E_d \rangle$, is related to T_{eff} as discussed above and previously [6, 10, 11], but the relationship is non-linear (see section on "Effective Temperature versus Internal Energy" or Figure 3a in Drahos and Vékey [11]) and the magnitudes of T_{eff} and

$\langle E_d \rangle$ depend on the molecular and instrumental parameters of the system (well-depth, size, frequencies, and time window). Therefore, the relationship between $\Delta\Delta S^{(y)}_{app}$ and T_{eff} is not meaningful in a thermodynamic sense.

In real experiments, one cannot make measurements of $\ln(I_2/I_1)$ at exactly $\Delta\Delta E_0 = 0$ to find the intercepts and obtain $\Delta\Delta S^{(y)}_{app}$. The simulation in Figure 9b shows that the apparent entropy obtained from the *y*-intercept from the linear regression, $\Delta\Delta S_{app} = +3.3$ J mol^{-1} K^{-1} for $T_s = 1000$ K, overestimates the actual *y*-intercepts for the heterodimers in Figure 9a when $\Delta\Delta E_0$ is artificially set to zero, for which $\Delta\Delta S^{(y)}_{app} = -3.7$ to $+2.1$ J mol^{-1} K^{-1} in the individual simulations. This deviation is a result of the variation of the slope and curvature for different cluster ions, and is another reason for caution in interpreting the apparent entropies. On the other hand, all of the $\Delta\Delta S_{app}$ terms are small for that simulation.

Extended Kinetic Method

In the extended kinetic method [4, 16–20], the measurements are carried out under several different conditions to change the effective temperature and then an apparent entropy change is determined by treating the effective temperature as a thermodynamic temperature. Various techniques have been used to vary the effective temperatures including comparing metastable dissociation with collision-induced dissociation (CID), CID with different target gases, changing the scattering detection angle in high-energy CID, or using different instruments. Within the present model, the effective temperature can be conveniently changed by using different instrumental time windows (analogous to using different instruments for metastable ion experiments). Figure 11a shows simulated kinetic plots for the $tBuO^-$(tBuOH) complex for various time windows with the vibrational frequencies of channel 2 scaled by 90%. Figure 11b compares the apparent entropies, $\Delta\Delta S^{(y)}_{app}$, with the statistical mechanical entropies $\Delta\Delta S^{\ddagger}(T = T_{eff})$. The thermodynamic entropy of activation difference $\Delta\Delta S^{\ddagger}(T)$ is about 2.5 times higher than the apparent entropies from the simulations, $\Delta\Delta S^{(y)}_{app}$.

Figure 11c reproduces the full entropy analysis of the extended kinetic method as prescribed by Armentrout [21]. Figure 11c is a plot of $\Delta\Delta S^{(y)}_{app} \equiv \Delta\Delta G_{app}/RT_{eff}$, the *y*-intercepts in Figure 11a, versus $1/RT_{eff}$, which is the negative of the slopes calculated as the tangents at $\Delta\Delta E = 0$. The average ion affinity of the reference compounds as defined in reference [21] corresponds to $\Delta\Delta H = 0$ here. The intercept of this plot is $\Delta\Delta S^{(\infty)}_{app}/R$, defining the apparent entropy difference, and the slope is $-\Delta\Delta H$. Results of simulations with source temperatures 300 and 600 K in addition to 1000 K are shown in Figure 11c; these represent a different way of changing the effective temperature (over smaller ranges) besides varying the time window. A technical advantage of the full entropy analysis is that it eliminates the dependence of $\Delta\Delta S^{(y)}_{app}$ on the effective temperature by extrapolating to $1/RT_{eff} = 0$ or $T_{eff} \rightarrow \infty$, hence the designation $\Delta\Delta S^{(\infty)}_{app}$. However, there are several difficulties with the interpretation of this extrapolated apparent entropy: (1) The procedure conceptually treats the effective temperature as a thermodynamic temperature, which it is not. (2) The values of $\Delta\Delta S^{(y)}_{app}$ are not approximately equal to the thermodynamic entropy of activation differences, $\Delta\Delta S^{\ddagger}(T)$, as shown above. (3) The plot in Figure 11c shows obvious curvature, so that $\Delta\Delta S^{(\infty)}_{app}$ depends on the range of time windows in the simulated experiments. This is also shown by the different lines obtained for the three source temperatures. (4) In Figure 11c, the extrapolated value of $\Delta\Delta S^{(\infty)}_{app} = 16.5$ J mol^{-1} K^{-1} for $T_s = 1000$ K matches $\Delta\Delta S^{\ddagger}(T)$ at $T \approx 279$ K, but that temperature has no obvious significance. The corresponding temperatures for the $T_s = 300$ and 600 K simulations are 239 and 270 K, respectively. The extrapolated value of $\Delta\Delta S^{(\infty)}_{app}$ must equal $\Delta\Delta S^{\ddagger}(T)$ at some temperature, simply because $\Delta\Delta S^{\ddagger}(T)$ varies with temperature. (5) The slope of the plot should equal zero because in the simulation the average gas phase acidity is taken as equal to the unknown. The actual slope in Figure 11c gives an apparent error of 2.7 kJ/mol for $T_s = 1000$ K, but this also will depend on the range of T_{eff} used in the simulations (the corresponding errors are 2.0 kJ/mol and 2.5 kJ/mol for the 300 K and 600 K source temperatures). On the basis of these observations, I conclude that the extrapolated apparent entropies obtained by the full entropy analysis of the extended kinetic method are of dubious physical significance. Furthermore, it is not obvious that the full entropy analysis provides an improvement in measured ion affinities over the isentropic kinetic method analysis, but that issue would require additional investigation.

Using RRKM theory and finite heat bath theory, Laskin and Futrell [9] obtained better agreement between $\Delta\Delta S^{(\infty)}_{app}$ and the statistical mechanics entropy of activation $\Delta\Delta S^{\ddagger}$ for their model reactions (although it is unclear what temperature they use for $\Delta\Delta S^{\ddagger}$). The different conclusions could be due to the differences in the statistical theory and kinetic model (see section on "Relationship to Previous Work"), or due to a coincidence from their choice of time windows or temperature for evaluation of $\Delta\Delta S^{\ddagger}$. It also appears that the larger of the cluster ions studied by Laskin and Futrell (up to 500 degrees of freedom) behave more like equilibrium systems than do small species.

Conclusions

Kinetic method experiments using metastable ion dissociation have been simulated using rigorous RRKM statistical rate theory. The simulations largely confirm the qualitative, relative dependence of the effective temperature on molecular and instrumental parameters (well-depth, size, and time window) as found by pre-

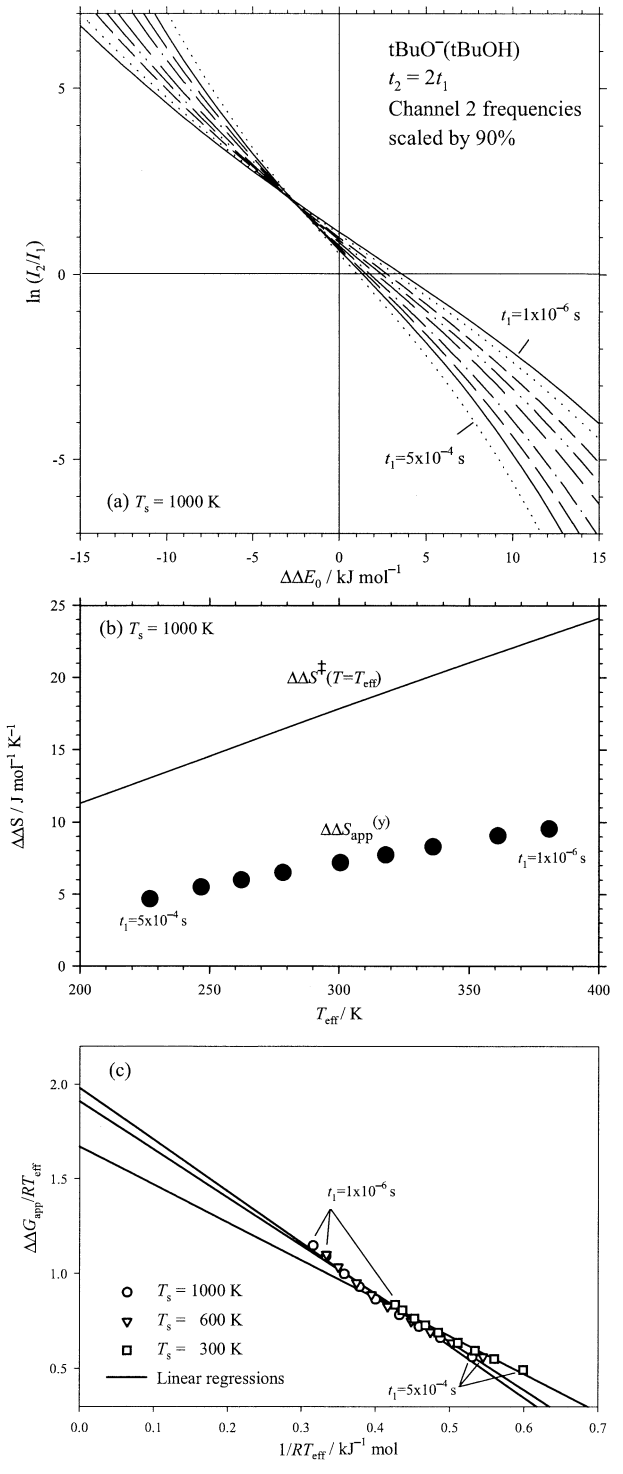

Figure 11. (**a**) Numerical simulation of kinetic method plots for model tert-butoxide/tert-butanol complexes with the vibrational frequencies of the second dissociation channel scaled by 90 %. Various time windows are used to change the effective temperatures. In sequence, the times are $t_1 = 1 \times 10^{-6}$ s, 2×10^{-6} s, 5×10^{-6} s, 1×10^{-5} s, 2×10^{-5} s, 5×10^{-5} s, 1×10^{-4} s, 2×10^{-4} s, and 5×10^{-4} s, with $t_2 = 2t_1$. The ion source temperature is 1000 K. (**b**) Comparisons of the apparent entropies (solid circles) obtained from the *y*-intercepts in part (**a**) with the thermodynamic entropy difference (line) calculated using statistical mechanics at a temperature equal to the effective temperature. (**c**) Full entropy analysis plots for source temperatures of 300, 600, and 1000 K (see text).

vious treatments [6–9, 11] and given by the approximate analytical expression, eq 13, derived previously using the classical RRK model [10]. Kinetic method plots of $\ln(I_2/I_1)$ versus $\Delta\Delta H$ are nearly linear, but can exhibit significant curvature. The curvature is most pronounced for cluster ions that dissociate rapidly—due to shallow wells or small sizes—relative to the instrumental time window. For these systems, the kinetically selected internal energies are near the dissociation thresholds. The effect of the variation effective temperature and curvature effects can lead to systematic errors in $\Delta\Delta H$ measurements by the kinetic method. The simulations imply that the accuracy of the thermochemical results may be limited by a ± 20 to $\pm 50\%$ variation in T_{eff} for individual $\Delta\Delta H$ determinations. The actual variation will depend on the systems of interest, but cannot necessarily be predicted without detailed modeling. Because of the ease of use, broad applicability, high sensitivity to small thermochemical differences (typically as small as 0.4 kJ/mol [2]), and high precision of the kinetic method, systematic deviations of that order of magnitude may be quite acceptable as long as they are recognized. As pointed out by Cooks et al. [4], because kinetic method experiments measure small differences in thermochemical affinities, large relative variation in T_{eff} may still lead to small absolute errors in ion affinities compared with other thermokinetic methods. For example, with the typical value $T_{eff} \approx 320$ K for the model systems in this work and a measured intensity ratio of $I_2/I_1 = 10$, a 20 –50% error in T_{eff} results in an absolute error of 1.2–3.1 kJ/mol. Calibrations involving multiple reference compounds might reduce the errors, or might not, depending on correlations between ion affinities and size or well-depth.

The apparent entropy term in kinetic method measurements is *not* approximately equal to the thermodynamic entropy of activation difference in general, either at the effective temperature or at any fixed temperature. Its magnitude relative to the thermodynamic entropy difference varies according to kinetic and system-dependent parameters. For metastable ion dissociation, a narrow slice of the ion energies is kinetically selected by the narrow time window of the experiment, so the distribution of internal energies of dissociating ions is closer to a single internal energy (microcanonical ensemble at energy E_d) than to a Boltzmann distribution (macrocanonical ensemble at a thermodynamic temperature T). The apparent entropy is approximately related to the ratio of the microcanonical sum of states for the two dissociation transition states evaluated at the mean internal energy of dissociating ions as given by eq 24. The mean internal energy is in turn related non-linearly to the effective temperature.

The present results apply to metastable ion dissociation experiments. For collision-induced dissociation, the internal energy distribution of dissociating ions is broader, but it is still non-Boltzmann. Energy-resolved competitive threshold collision-induced dissociation experiments have demonstrated that precise and accurate

thermochemical results are best obtained with a full RRKM statistical rate model to account and correct for entropic effects as a function of energy [13, 35, 36]. The choice of the model systems also influence the quantitative results reported here, which therefore apply to species with similar sizes and frequency distributions as the model alkanols.

Acknowledgments

This work was supported by the U.S. Department of Energy, Basic Energy Sciences Office, Chemical Sciences, Geosciences, and Biosciences Division. The author thanks Professor Graham Cooks, Professor Peter Armentrout, and anonymous referees for helpful suggestions.

References

1. McLuckey, S. A.; Cameron, D.; Cooks, R. G. Proton Affinities from Dissociations of Proton-Bound Dimers. *J. Am. Chem. Soc.* **1981,** *130,* 1313–1317.
2. Cooks, R. G.; Patrick, J. S.; Kotiaho, T.; McLuckey, S. A. Thermochemical Determinations by the Kinetic Method. *Mass Spectrom. Rev.* **1994,** *13,* 287–339.
3. Cooks, R. G.; Wong, P. S. H. Kinetic Method of Making Thermochemical Determinations: Advances and Applications. *Acc. Chem. Res.* **1998,** *31,* 379–386.
4. Cooks, R. G.; Koskinen, J. T.; Thomas, P. D. The Kinetic Method of Making Thermochemical Determinations. *J. Mass Spectrom.* **1999,** *34,* 85–92.
5. Grützmacher, H.-F.; Caltapanides, A. Dissociation of Proton-Bound Complexes and Proton Affinities of Benzamides. *J. Am. Soc. Mass Spectrom.* **1994,** *5,* 826–836.
6. Bojesen, G.; Breindahl, T. On the Proton Affinity of Some α-Amino Acids and the Theory of the Kinetic Method. *J. Chem. Soc. Perkin Trans.* **2,** *1994,* 1029–1037.
7. Campbell, S.; Marzluff, E. M.; Rodgers, M. T.; Beauchamp, J. L.; Rempe, M. E.; Schwinck, K. F.; Lichtenberger, D. L. Proton Affinities and Photoelectron Spectra of Phenylalanine and N-Methyl and N,N-Dimethylphenyalanine. Correlation of Lone Pair Ionization Energies with Proton Affinities and Implications for N-Methylation as a Method to Effect Site Specific Protonation of Peptides. *J. Am. Chem. Soc.* **1994,** *116,* 5257–5264.
8. Craig, S. L.; Zhong, M.; Choo, B.; Brauman, J. I. Branching Ratios in Activated Systems. *J. Phys. Chem. A* **1997,** *101,* 19–24.
9. Laskin, J.; Futrell, J. H. The Theoretical Basis of the Kinetic Method from the Point of View of Finite Heat Bath Theory. *J. Phys. Chem. A* **2000,** *104,* 8829–8837.
10. Ervin, K. M. Microcanonical Analysis of the Kinetic Method. The Meaning of the "Effective Temperature". *Int. J. Mass Spectrom.* **2000,** *195/196,* 271–284.
11. Drahos, L.; Vékey, K. How Closely Related Are the Effective and the Real Temperature? *J. Mass Spectrom.* **1999,** *34,* 79–84.
12. Drahos, L.; Vékey, K. Mass Kinetics: A Theoretical Model of Mass Spectra Incorporating Physical Processes, Reaction Kinetics, and Mathematical Descriptions. *J. Mass Spectrom.* **2001,** *36,* 237–263.
13. Armentrout, P. B. Is the Kinetic Method a Thermodynamic Method? *J. Mass Spectrom.* **1999,** *34,* 74–78.
14. Holmes, J. L.; Aubry, C.; Mayer, P. M. Proton Affinities of Primary Alkanols: An Appraisal of the Kinetic Method. *J. Phys. Chem. A* **1999,** *103,* 705–709. Erratum, *ibid.* **1999**, *103*, 6492.
15. Thomas, P. D.; Cooks, R. G.; Vékey, K.; Drahos, L. Comments on "Proton Affinities of Primary Alkanols: An Appraisal of the Kinetic Method". *J. Phys. Chem. A* **2000,** *104,* 1359–1361.
16. Cheng, X.; Wu, Z.; Fenselau, C. Collision Energy Dependence of Proton-Bound Dimer Dissociation: Entropy Effects, Proton Affinities, and Intramolecular Hydrogen-Bonding in Protonated Peptides. *J. Am. Chem. Soc.* **1993,** *115,* 4844–4848.
17. Wu, Z.; Fenselau, C. Gas-Phase Basicities and Proton Affinities of Lysine and Histidine Measured from the Dissociation of Proton-Bound Dimers. *Rapid Commun. Mass Spectrom.* **1994,** *8,* 777–780.
18. Cerda, B. A.; Wesdemiotis, C. Li^+, Na^+, and K^+ Binding to the DNA and RNA Nucleobases. Bond Energies and Attachment Sites from the Dissociation of Metal Ion-Bound Heterodimers. *J. Am. Chem. Soc.* **1996,** *118,* 11884–11892.
19. Cerda, B. A.; Hoyau, S.; Ohanessian, G.; Wesdemiotis, C. Na^+ Binding to Cyclic and Linear Dipeptides. Bond Energies, Entropies of Na^+ Complexation, and Attachment Sites from the Dissociation of Na^+-Bound Heterodimers and ab Initio Calculations. *J. Am. Chem. Soc.* **1998,** *120,* 2437–2448.
20. Cerda, B. A.; Wesdemiotis, C. Gas Phase Copper(I) Ion Affinities of Valine, Lysine, and Arginine Based on the Dissociation of Cu^+-Bound Heterodimers at Varying Internal Energies. *Int. J. Mass Spectrom.* **1999,** *185/186/187,* 107–116.
21. Armentrout, P. B. Entropy Measurements and the Kinetic Method: A Statistically Meaningful Approach. *J. Am. Soc. Mass Spectrom.* **2000,** *11,* 371–379.
22. Wenthold, P. G. Determination of the Proton Affinities of Bromo- and Iodoacetonitrile Using the Kinetic Method with Full Entropy Analysis. *J. Am. Soc. Mass Spectrom.* **2000,** *11,* 601–605.
23. Lardin, H. A.; Squires, R. R.; Wenthold, P. G. Determination of the Electron Affinities of the α- and β-Naphthyl Radicals Using the Kinetic Method with Full Entropy Analysis. The C–H Bond Dissociation Energies of Naphthalene. *J. Mass Spectrom.* **2001,** *36,* 607–615.
24. Williams, T. I.; Denault, J. W.; Cooks, R. G. Proton Affinity of Deuterated Acentonitrile Estimated by the Kinetic Method with Full Entropy Analysis. *Int. J. Mass Spectrom.* **2001,** *210/211,* 133–146.
25. Di Donna, L.; Napoli, A.; Sindona, G. Entropy Effect in the Evaluation of the Proton Affinity of N-3-Benzoyl-2-Dioxycytidines by the Kinetic Method. *Int. J. Mass Spectrom.* **2001,** *210/211,* 165–172.
26. Kuntz, A. F.; Boynton, A. W.; David, G. A.; Colyer, K. E.; Poutsma, J. C. The Proton Affinity of Proline Analogs Using the Kinetic Method with Full Entropy Analysis. *J. Am. Soc. Mass Spectrom.* **2002,** *13,* 72–81.
27. Gilbert, R. G.; Smith, S. C. *Theory of Unimolecular and Recombination Reactions.* Blackwell Scientific: Boston, 1990, pp 52–208.
28. Baer, T.; Hase, W. L. *Unimolecular Reaction Dynamics: Theory and Experiments.* Oxford University Press: New York, 1996, pp 171–264.
29. Steinfeld, J. I.; Francisco, J. S.; Hase, W. L. *Chemical Kinetics and Reaction Dynamics; 2nd ed.* Prentice-Hall: Upper Saddle River, 1998, pp 287–377.
30. Waage, E. V.; Rabinovitch, B. S. Centrifugal Effects in Reaction Rate Theory. *Chem. Rev.* **1970,** *70,* 377–387.
31. Rodgers, M. T.; Ervin, K. M.; Armentrout, P. B. Statistical Modeling of Collision-Induced Dissociation Thresholds. *J. Chem. Phys.* **1997,** *106,* 4499–4508.
32. Winn, J. S. *Physical Chemistry.* Harper Collins College Publishers: New York, 1995, (a) p 130, (b) p 90.
33. Baer, T.; Mayer, P. M. Statistical Rice-Ramsperger-Kassel-Marcus Quasiequilibrium Theory Calculations in Mass Spectrometry. *J. Am. Soc. Mass Spectrom.* **1997,** *8,* 103–115.
34. Truhlar, D. G.; Garret, B. C.; Klippenstein, S. J. Current Status of Transition-State Theory. *J. Phys. Chem.* **1996,** *100,* 12771–12800.

35. Rodgers, M. T.; Armentrout, P. B. Statistical Modeling of Competitive Threshold Collision-Induced Dissociation. *J. Chem. Phys.* **1998,** *109,* 1787–1800.
36. DeTuri, V. F.; Ervin, K. M. Competitive Threshold Collision-Induced Dissociation: Gas Phase Acidities and Bond Dissociation Energies for a Series of Alcohols. *J. Phys. Chem. A* **1999,** *103,* 6911–6920.
37. Armentrout, P. B.; Ervin, K. M. *CRUNCH*; Fortran program.
38. Beyer, T. S.; Swinehart, D. F. Number of Multiply-Restricted Partitions. *Commun. ACM* **1973,** *16,* 379.
39. Stein, S. E.; Rabinovitch, B. S. Accurate Evaluation of the Internal Energy Level Sums and Densities Including Anharmonic Oscillators and Hindered Rotors. *J. Chem. Phys.* **1973,** *58,* 2438–2445.
40. Stein, S. E.; Rabinovitch, B. S. On the Use of Exact State Counting Methods in RRKM Rate Calculations. *Chem. Phys. Lett.* **1977,** *49,* 183–188.
41. Frisch, M. J.; Trucks, G. W.; Schlegel, H. B.; Scuseria, G. E.; Robb, M. A.; Cheeseman, J. R.; Zakrzewski, V. G.; Montgomery, J. A., Jr.; Stratmann, R. E.; Burant, J. C.; Dapprich, S.; Millam, J. M.; Daniels, A. D.; Kudin, K. N.; Strain, M. C.; Farkas, O.; Tomasi, J.; Barone, V.; Cossi, M.; Cammi, R.; Mennucci, B.; Pomelli, C.; Adamo, C.; Clifford, S.; Ochterski, J.; Petersson, G. A.; Ayala, P. Y.; Cui, Q.; Morokuma, K.; Malick, D. K.; Rabuck, A. D.; Raghavachari, K.; Foresman, J. B.; Cioslowski, J.; Ortiz, J. V.; Stefanov, B. B.; Liu, G.; Liashenko, A.; Piskorz, P.; Komaromi, I.; Gomperts, R.; Martin, R. L.; Fox, D. J.; Keith, T.; Al-Laham, M. A.; Peng, C. Y.; Nanayakkara, A.; Gonzalez, C.; Challacombe, M.; Gill, P. M. W.; Johnson, B.; Chen, W.; Wong, M. W.; Andres, J. L.; Head-Gordon, M.; Replogle, E. S.; Pople, J. A. *Gaussian 98 Revision A.6.* Gaussian, Inc.: Pittsburgh, PA, 1998.
42. Higgins, P. R.; Bartmess, J. E. The Gas-Phase Acidities of Long Chain Alcohols. *Int. J. Mass Spectrom. Ion Processes* **1998,** *175,* 71–79.
43. Scott, A. P.; Radom, L. Harmonic Vibrational Frequencies: An Evaluation of Hartree-Fock, Møller-Plesset, Quadratic Configuration Interaction, Density Functional Theory, and Semiempirical Scale Factors. *J. Phys. Chem.* **1996,** *100,* 16502–16513.
44. Miller, T. M. Atomic and Molecular Polarizabilities. *In Handbook of Chemistry and Physics;* Lide, D. R., Ed.; CRC Press: Boca Raton, 1990; 10/193–10/209.
45. Bartmess, J. E. Negative Ion Energetics Data. In *NIST Chemistry WebBook, NIST Standard Reference Database Number 69*; Mallard, W. G.; Linstrom, P. J., Eds.; National Institute of Standards and Technology: Gaithersburg, MD, July 2001; (http://webbook.nist.gov).
46. DeTuri, V. F.; Su, M. A.; Ervin, K. M. Dynamics of Endoergic Bimolecular Proton Transfer Reactions: $F^- + ROH \rightarrow HF + RO^-$ (R = H, CH_3, CH_3CH_2, $(CH_3)_2CH$, and $(CH_3)_3C$). *J. Phys. Chem. A* **1999,** *103,* 1468–1479.
47. Boand, G.; Houriet, R.; Gäumann, T. Gas-Phase Acidities of Aliphatic Alcohols. *J. Am. Chem. Soc.* **1983,** *105,* 2203–2206.
48. Majumdat, T. K.; Clairet, F.; Tabet, J.-C.; Cooks, R. G. Epimer Distinction and Structural Effects on Gas Phase Acidities of Alcohols Measured Using the Kinetic Method. *J. Am. Chem. Soc.* **1992,** *114,* 2897–2903.
49. Haas, M. J.; Harrison, A. G. The Fragmentation of Proton-Bound Cluster Ions and the Gas-Phase Acidities of Alcohols. *Int. J. Mass Spectrom. Ion Processes* **1993,** *124,* 115–124.
50. Meot-Ner (Mautner), M.; Lias, S. G. Thermochemistry of Cluster Ion Data. In *NIST Chemistry WebBook, NIST Standard Reference Database Number 69*; Mallard, W. G.; Linstrom, P. J., Eds.; National Institute of Standards and Technology: Gaithersburg, MD, July 2001; (http://webbook.nist.gov).
51. Shvartsburg, A. A.; Ervin, K. M.; Frederick, J. H. Models for Statistical Decomposition of Metal Clusters: Vibrational Frequency Distributions. *J. Chem. Phys.* **1996,** *104,* 8458–8469.
52. Wenthold, P. G.; Squires, R. R. Gas-Phase Properties and Reactivity of the Acetate Radical Anion. Determination of the C–H Bond Strengths in Acetic Acid and Acetate Ion. *J. Am. Chem. Soc.* **1994,** *116,* 11890–11897.